

Supporting Information for

Thermally Activated Delayed Fluorescence Enantiomers for Solution-processed Circularly Polarized Electroluminescence Devices

Sibing Sun, Jun Wang, Lingfeng Chen, Runfeng Chen, Jibiao Jin, Cailin Chen,*

Shufen Chen, Guohua Xie, Chao Zheng, Wei Huang**

Key Laboratory for Organic Electronics and Information Displays & Jiangsu Key Laboratory for Biosensors, Institute of Advanced Materials (IAM), Jiangsu National Synergistic Innovation Center for Advanced Materials (SICAM), Nanjing University of Posts & Telecommunications, 9 Wenyuan Road, Nanjing 210023, China

E-mail: iamrfchen@njupt.edu.cn; iamwhuang@njtech.edu.cn

Prof. G. Xie

Sauvage Center for Molecular Sciences, Hubei Key Lab on Organic and Polymeric Optoelectronic Materials, Department of Chemistry, Wuhan University, Wuhan, 430072, China.

E-mail: guohua.xie@whu.edu.cn

Table of contents

1. Instrumentation and Materials	2
2. Synthesis scheme and process	3
3. Chiral high-performance liquid chromatography (HPLC) Analysis	15
4. Thermal properties	16
5. Theoretical calculations	16
6. Morphology properties	17
7. Photophysical properties	18
8. Electrochemical properties	20
9. Thermally activated delayed fluorescence organic light emitting diode (TADF OLED) devices fabrication	21
10. CPL and CPEL performance	25
11. A summary of CP-OLEDs	28

1. Instrumentation and materials

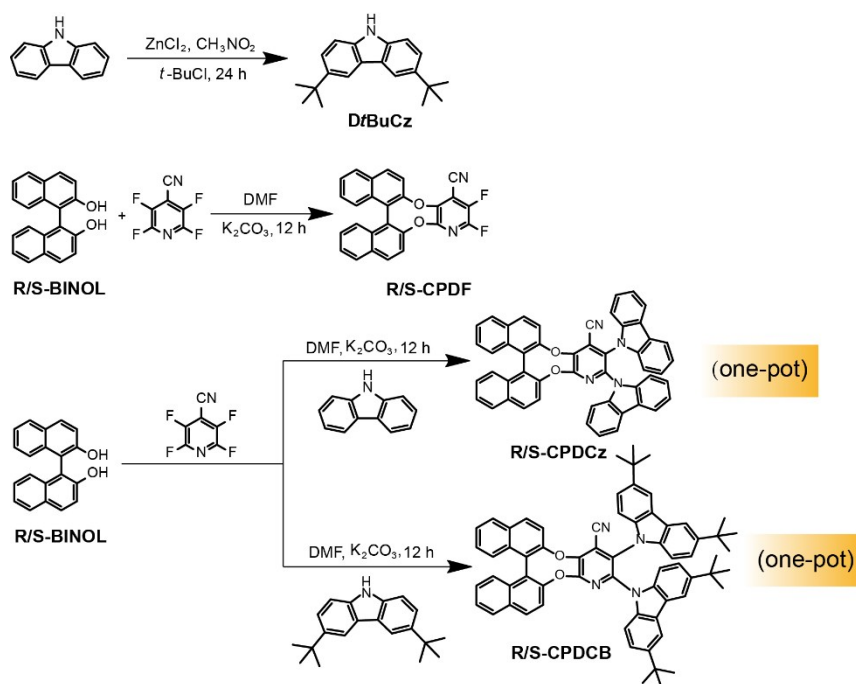
1.1 Materials

Chemical reagents, unless otherwise specified, were purchased from Energy Chemical, Acros, or Alfa Aesar, and used without further purification. Manipulations involving air-sensitive reagents were performed in an atmosphere of dry argon. 3,6-di-*tert*-butyl-9H-carbazole (**DtBuCz**) was synthesized according to the reported procedures.^[1]

1.2 Instruments

¹H and ¹³C-nuclear magnetic resonance (NMR) spectra were recorded on a Bruker Ultra Shield Plus 400 MHz instrument with CDCl₃ as the solvent and tetramethylsilane (TMS) as the internal standard. In the nuclear magnetic resonance spectra, *m* represents multiple peaks, *s* represents a single peak, *d* represents a doublet peaks, *t* represents a triplet peaks and *q* represents a quadruple peaks. High resolution mass spectra (HRMS) were obtained on an LCT Premier XE (Waters) HRMS spectrometry. Circular dichroism (CD) spectra were recorded with a Chirascan spectrometer (Applied Photophysics, England). Circularly polarized luminescence (CPL) spectra of the films and solution were recorded at a 50 nm min⁻¹ scan speed with a commercialized instrument of JASCO CPL-300 at room temperature. Circularly polarized electroluminescence (CPEL) spectra were also recorded on JASCO CPL-300 at room temperature under a driving voltage of 9.0 V.

2. Synthesis and characterization



Scheme S1. Synthesis of **R-/S-CPDCz** and **R-/S-CPDCB**.

3,6-Di-tert-butyl-9H-carbazole (**DfBuCz**)

Carbazole (10.0 g, 59.9 mmol), anhydrous aluminum chloride (8.0 g, 60 mmol), and dichloromethane (200 mL) were placed in a 500 mL three-necked flask and stirred until complete dissolution. After the mixture was cooled to 0°C , chloro-*tert*-butane (6.6 mL, 60 mmol) in dichloromethane (20 mL) was added dropwise. The reaction solution was allowed to be stirred at 0°C for 15 min, then at room temperature for 4.0 h. The reaction was quenched by pouring into water (200 mL) and extracted with dichloromethane (3×100 mL). The organic phase was collected, combined, and dried over anhydrous sodium sulfate. The solvent was removed under reduced pressure and the residue was separated by layer chromatography (ethyl acetate/petroleum ether = 1:5). The crude product was recrystallized from petroleum ether to give 9.6 g of white solid. ^1H NMR (400 MHz, $CDCl_3$): δ = 8.10 (*d*, 2H), 7.80 (*s*, 1H), 7.50-7.48 (*d*, J = 8 Hz, 2H), 7.37-7.35 (*d*, J = 8 Hz, 2H), 1.48 (*s*, 18H). ^{13}C NMR (100 MHz, $CDCl_3$): δ = 142.49, 142.25, 139.91, 137.58, 125.60, 123.88, 123.60, 123.05, 120.18, 119.23, 116.40, 116.22, 110.61, 110.11, 110.05, 34.74, 32.09, 32.05.

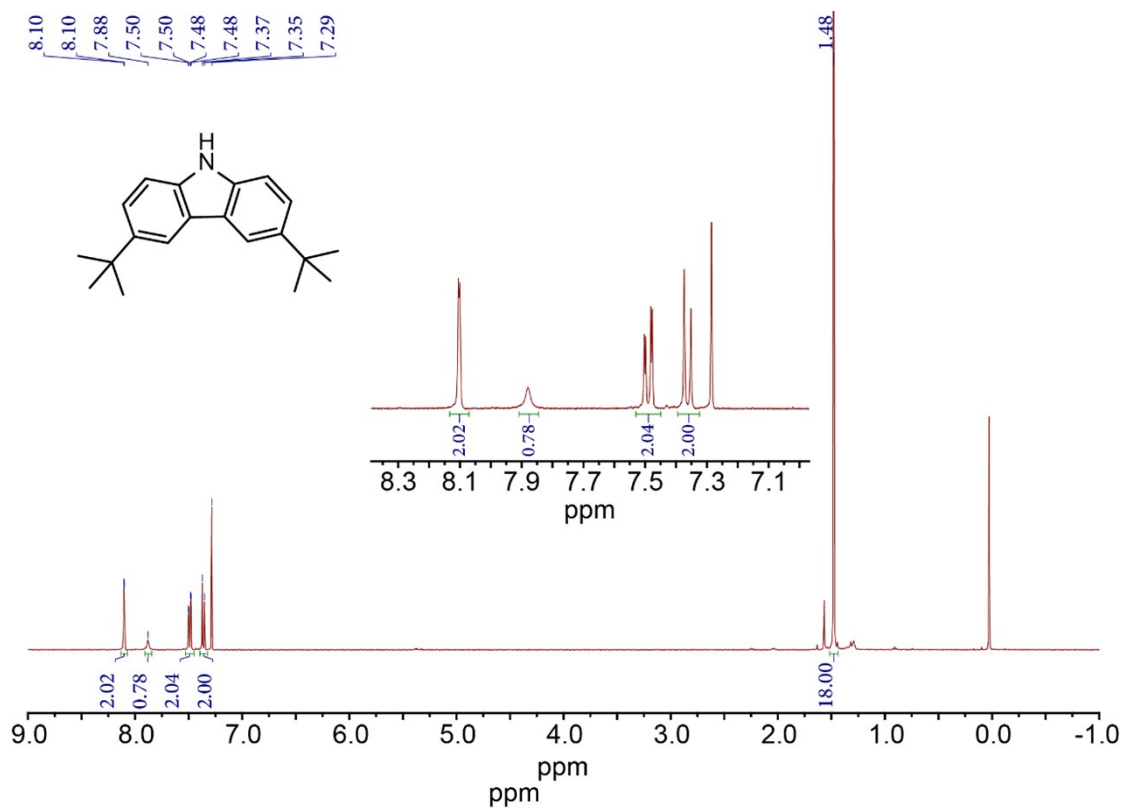


Figure S1. ^1H NMR spectrum of *DtBuCz* in CDCl_3 .

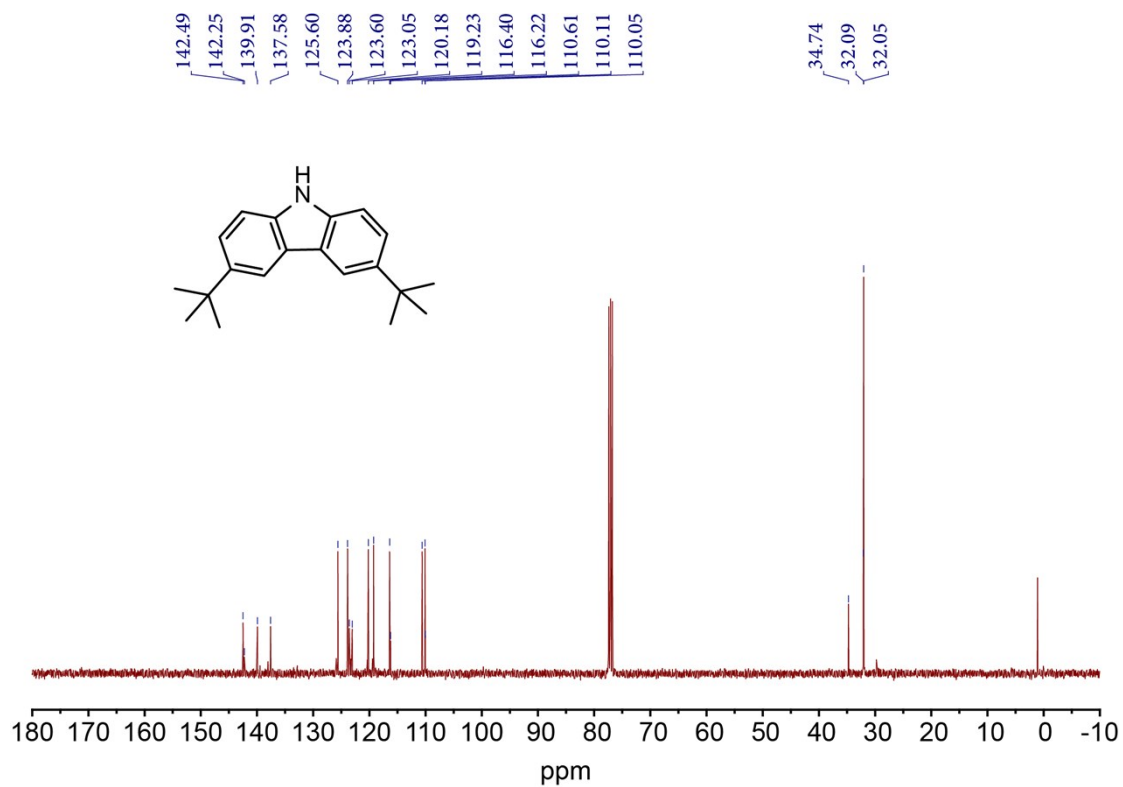


Figure S2. ^{13}C NMR spectrum of *DtBuCz* in CDCl_3 .

2,3-Di(9H-carbazol-9-yl)dinaphtho[2',1':5,6;1'',2'':7,8] [1,4]dioxocino[2,3-b]pyridine-4-carbonitrile (S-/R-CPDCz)

One-pot synthesis of the enantiomers of **S-CPDCz** and **R-CPDCz** were performed identically. Take **S-CPDCz** as an example. A mixture of [1,1'-binaphthalene]-2,2'-diol (**S-BINOL**) (1.6 g, 5.60 mmol), 2,3,5,6-tetrafluoropyridine-4-carbonitrile (1.0 g, 5.60 mmol), carbazole (2.1 g, 12.3 mmol) and K₂CO₃ (3.1 g, 22.40 mmol) were dissolved in anhydrous N,N-dimethylformamide (DMF) (50 mL). The mixture was stirred for 12 h at room temperature to complete the reaction. Then water (30 mL) was added into. The mixture was extracted with ethyl acetate (3×15 mL) and the organic layers were separated, collected, combined, and dried with anhydrous Na₂SO₄ and evaporated under reduced pressure to remove the solvents. The obtained residue was purified by silica gel column chromatography (petroleum ether/dichloromethane = 2:1) to yield 3.2 g (80%) of the product of **S-CPDCz** as a yellow powder after removal of the solvent. ¹H NMR (400 MHz, CDCl₃): δ = 8.19-8.14 (*t*, J = 12 Hz, 2H), 8.09-8.05 (*t*, J = 8.0 Hz, 2H), 7.88-7.86 (*d*, J = 8 Hz, 1H), 7.79-7.73 (*m*, 4H), 7.65-7.48 (*m*, 5H), 7.34-7.28 (*q*, J = 8 Hz, 3H), 7.36-7.30 (*q*, J = 8 Hz, 2H), 7.28-7.19 (*m*, 3H), 7.03-7.00 (*t*, J = 4 Hz, 2H), 6.87-6.83 (*t*, J = 8 Hz, 2H), 6.76-6.74 (*d*, J = 8 Hz, 2H). ¹³C NMR (100 MHz, CDCl₃): δ = 152.42, 149.41, 148.81, 144.70, 141.73, 139.01, 138.74, 138.22, 138.00, 132.48, 132.33, 132.21, 132.20, 131.65, 131.45, 128.60, 128.56, 127.71, 127.53, 127.46, 126.89, 126.73, 126.51, 126.40, 125.49, 125.21, 125.17, 125.13, 124.26, 124.21, 124.01, 123.91, 121.42, 121.32, 121.25, 121.11, 120.93, 120.86, 120.51, 120.07, 119.91, 119.70, 119.23, 111.44, 110.41, 109.93, 109.65, 109.46. Yield: 3.3 g of **R-CPDCz** in yellow powder (81%): ¹H NMR (400 MHz, CDCl₃): δ = 8.19-8.15 (*t*, J = 12 Hz, 2H), 8.09-8.05 (*t*, J = 8.0 Hz, 2H), 7.89-7.80 (*d*, J = 8 Hz, 1H), 7.79-7.74 (*m*, 4H), 7.65-7.49 (*m*, 5H), 7.35-7.33 (*q*, J = 8 Hz, 3H), 7.32-7.30 (*q*, J = 8 Hz, 2H), 7.28-7.19 (*m*, 3H), 7.03-6.88 (*t*, J = 4 Hz, 2H), 6.87-6.83 (*t*, J = 16 Hz, 2H), 6.82-6.80 (*d*, J = 8 Hz, 2H). ¹³C NMR (100 MHz, CDCl₃): δ = 149.45, 148.84, 144.74, 138.77, 138.26, 132.50, 132.35, 132.23, 131.68, 131.47, 128.62, 128.58, 127.75, 127.55, 127.49,

126.91, 126.75, 126.53, 126.43, 126.13, 125.52, 125.24, 125.16, 124.28, 124.04, 121.45, 121.27, 121.15, 120.88, 120.54, 120.11, 109.68, 109.50. HRMS (MALDI-TOF, m/z): [M]⁺ Na calcd for C₅₀H₂₈N₄O₂, 716.2212; found, 739.2115.

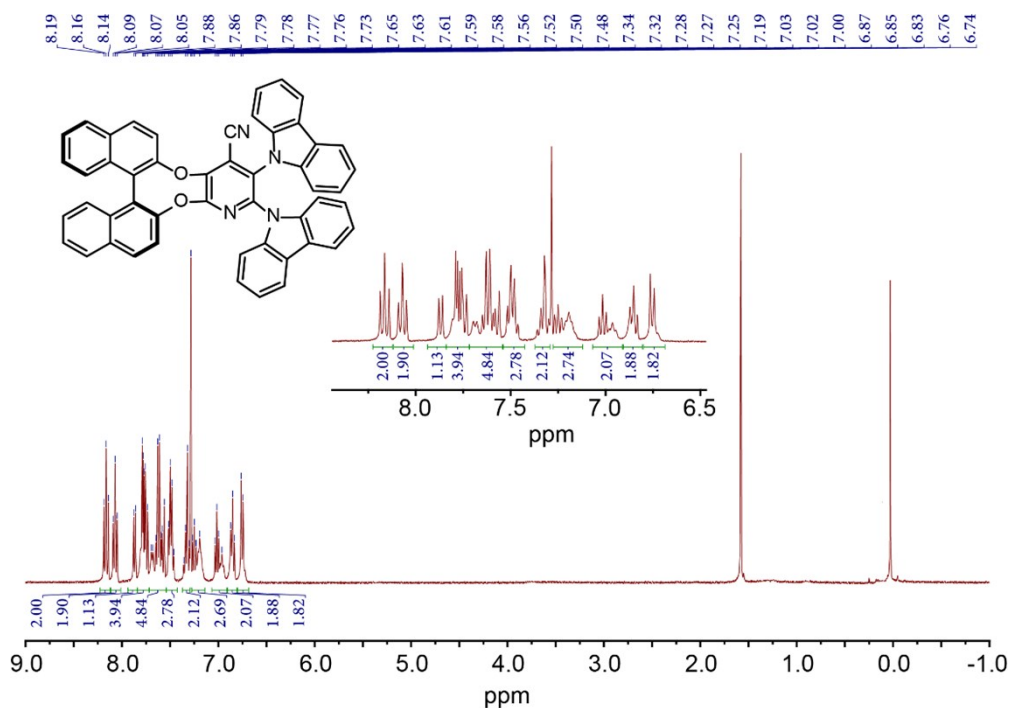


Figure S3. ¹H NMR spectrum of S-CPDCz in CDCl₃.

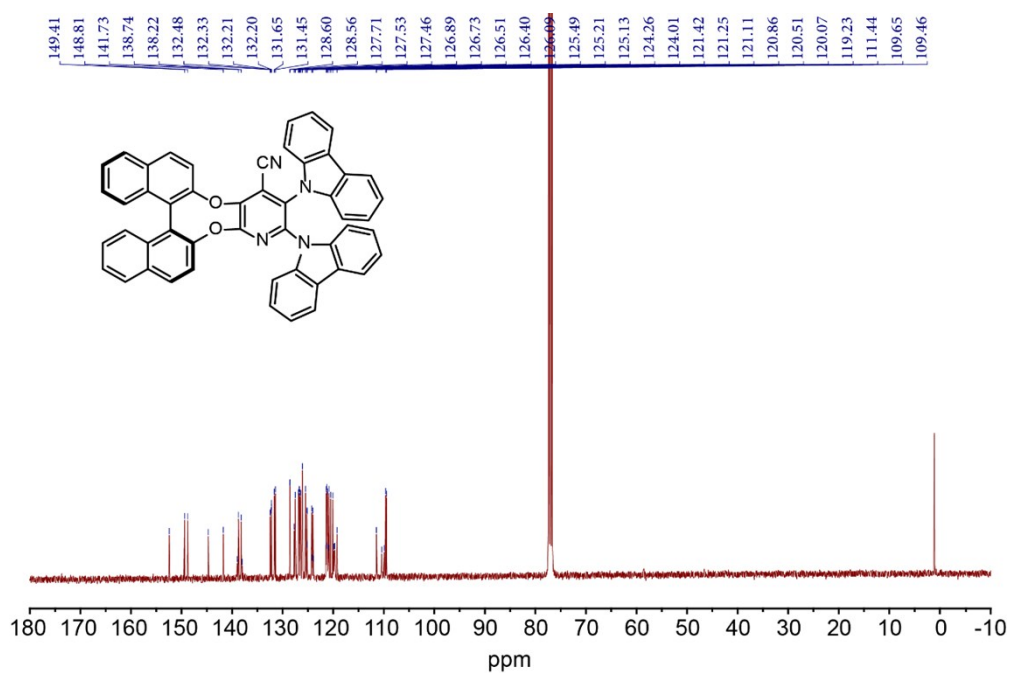


Figure S4. ¹³C NMR spectrum of S-CPDCz in CDCl₃.

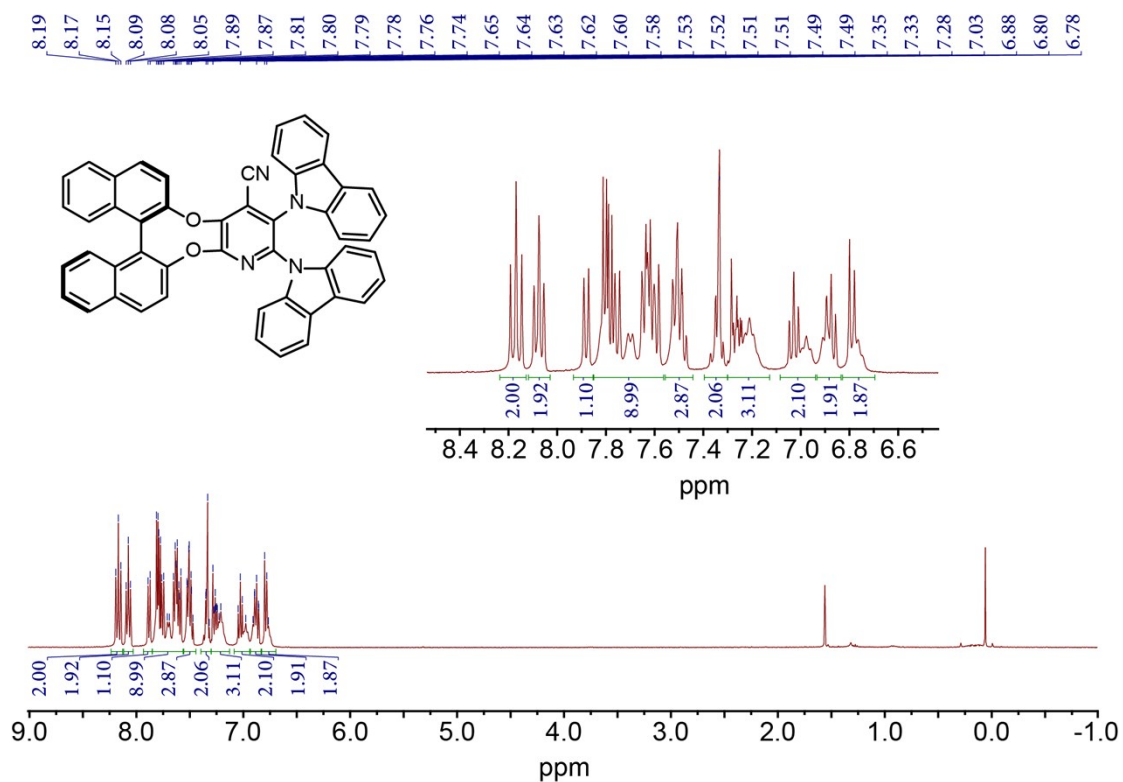


Figure S5. ^1H NMR spectrum of R-CPDCz in CDCl_3 .

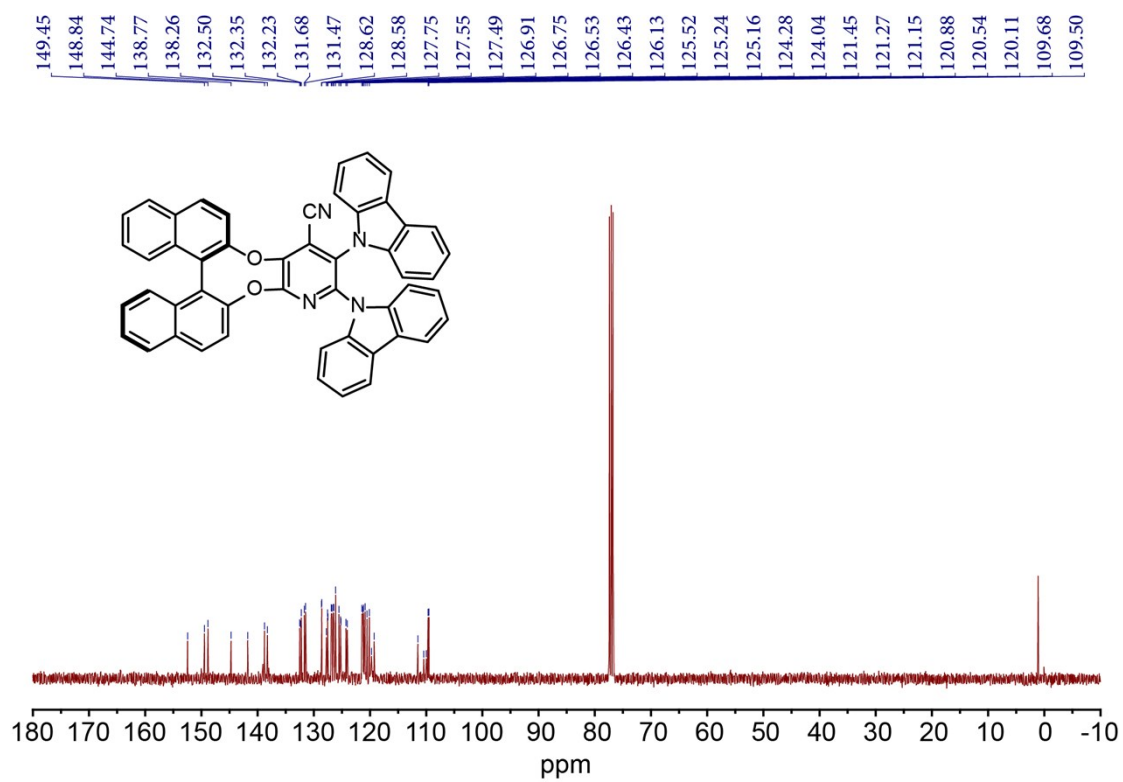


Figure S6. ^{13}C NMR spectrum of R-CPDCz in CDCl_3 .

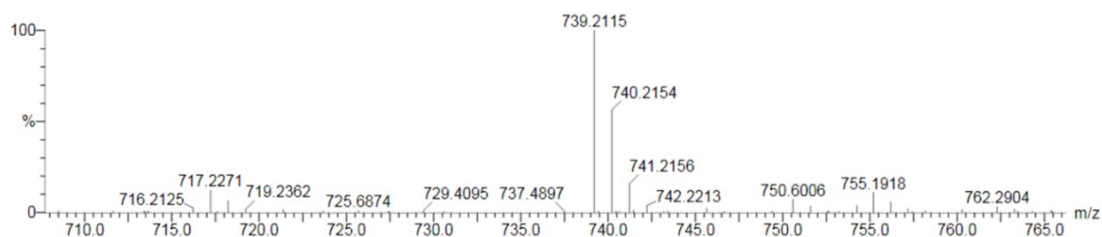


Figure S7. HRMS spectrum of **S-CPDCz**.

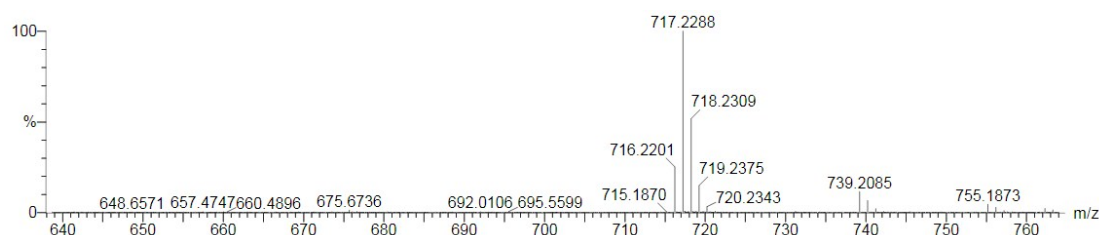


Figure S8. HRMS spectrum of **R-CPDCz**.

2,3-Bis(3,6-di-tert-butyl-9H-carbazol-9-yl)dinaphtho[2',1':5,6;1'',2'':7,8] [1,4] dioxocino[2,3-b]pyridine-4-carbonitrile (S-/R-CPDCB)

The enantiomers of **S-CPDCB** and **R-CPDCB** were synthesized identically in one-pot. Take **S-CPDCB** as an example. A mixture of [1,1'-binaphthalene]-2,2'-diol (**S-BINOL**) (1.6 g, 5.60 mmol), 2,3,5,6-tetrafluoropyridine-4-carbonitrile (1.0 g, 5.60 mmol), **DtBuCz** (3.4 g, 12.3 mmol) and K_2CO_3 (3.1 g, 22.4 mmol) were dissolved in anhydrous *N,N*-dimethylformamide (DMF) (50 mL). The mixture was stirred for 12 h at room temperature to complete the reaction. And then water (30 mL) was added. The mixture was extracted with ethyl acetate (3×15 mL). The combined organic layers were dried with anhydrous Na_2SO_4 and evaporated under reduced pressure to obtain the crude product. The residue was purified by silica gel column chromatography (petroleum ether/dichloromethane = 2:1) to yield 4.5 g (85%) of the product as a yellow powder after removal of the solvent. 1H NMR (400 MHz, $CDCl_3$): δ = 8.20-8.16 (*t*, *J* = 8.8 Hz, 2H), 8.10-8.06 (*t*, *J* = 8 Hz, 2H), 7.84-7.82 (*d*, *J* = 8 Hz, 2H), 7.66-7.58 (*m*, 6H), 7.53-7.48 (*q*, *J* = 8 Hz, 4H), 7.20-7.16 (*t*, *J* = 8 Hz, 2H), 7.05-7.03 (*d*, *J* = 8 Hz, 1H), 6.99-6.97 (*d*, *J* = 8 Hz, 1H), 6.72-6.70 (*d*, *J* = 8 Hz, 1H), 6.60 (*s*, 2H), 6.48-6.45 (*d*, *J* = 12 Hz, 1H), 1.32-1.29 (*d*, *J* = 12 Hz, 36H). ^{13}C NMR (100 MHz, $CDCl_3$): δ = 151.74, 149.58,

149.00, 144.02, 143.87, 143.75, 143.66, 141.96, 137.18, 137.09, 136.65, 132.44, 132.29, 132.24, 131.59, 131.40, 128.59, 128.55, 128.13, 127.45, 127.39, 126.91, 126.75, 126.41, 126.31, 123.2, 122.5, 121.2, 120.9, 120.74, 120.71, 120.06, 119.56, 116.3, 115.7, 114.56, 114.47, 112.06, 125.29, 125.21, 124.64, 124.49, 124.45, 124.18, 124.01, 123.37, 123.27, 122.86, 122.57, 122.53, 121.39, 120.99, 116.04, 115.46, 115.36, 115.02, 114.09, 111.91, 109.71, 109.54, 109.15, 34.63, 34.55, 34.44, 32.09, 31.95, 31.92, 31.85, 31.77, 31.46. Yield: 4.5 g of **R-CPDCB** in yellow powder (85%): ^1H NMR (400 MHz, CDCl_3): δ = 8.20-8.16 (*t*, J = 8.8 Hz, 2H), 8.10-8.06 (*t*, J = 8 Hz, 2H), 7.88-7.81 (*m*, J = 8 Hz, 2H), 7.66-7.57 (*m*, 6H), 7.53-7.48 (*q*, J = 8 Hz, 4H), 7.29-7.15 (*t*, J = 8 Hz, 2H), 7.02 (*s*, 1H), 6.98-6.96 (*d*, J = 8 Hz, 1H), 6.71-6.69 (*d*, J = 8 Hz, 1H), 6.60 (*s*, 2H), 6.47-6.45 (*d*, J = 8 Hz, 1H), 1.32-1.29 (*d*, J = 12 Hz, 36H). ^{13}C NMR (100 MHz, CDCl_3): δ = 144.59, 142.24, 138.05, 132.36, 131.75, 131.52, 128.58, 127.49, 126.83, 126.70, 126.45, 125.57, 124.19, 124.13, 123.84, 123.54, 123.34, 120.44, 120.16, 119.22, 116.90, 116.38, 116.20, 110.57, 110.07, 110.01, 34.87, 34.84, 34.72, 32.06, 32.02, 31.98, 31.96. HRMS (MALDI-TOF, m/z): $[\text{M}]^+ \text{Na}$ calcd for $\text{C}_{66}\text{H}_{60}\text{N}_4\text{O}_2$, 940.4716; found, 963.4614.

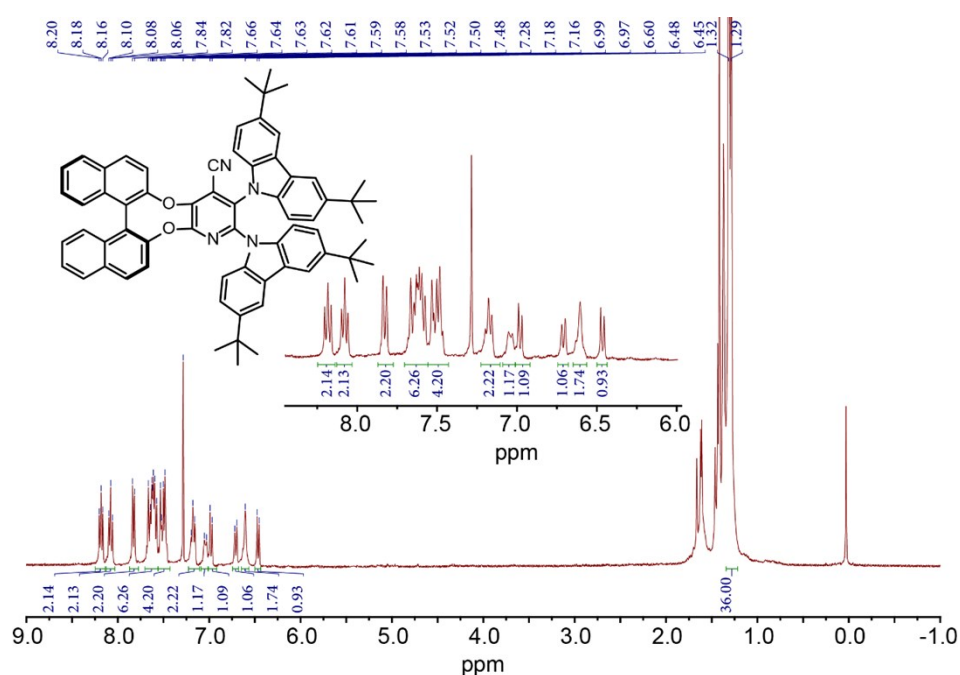


Figure S9. ^1H NMR spectrum of **S-CPDCB** in CDCl_3 .

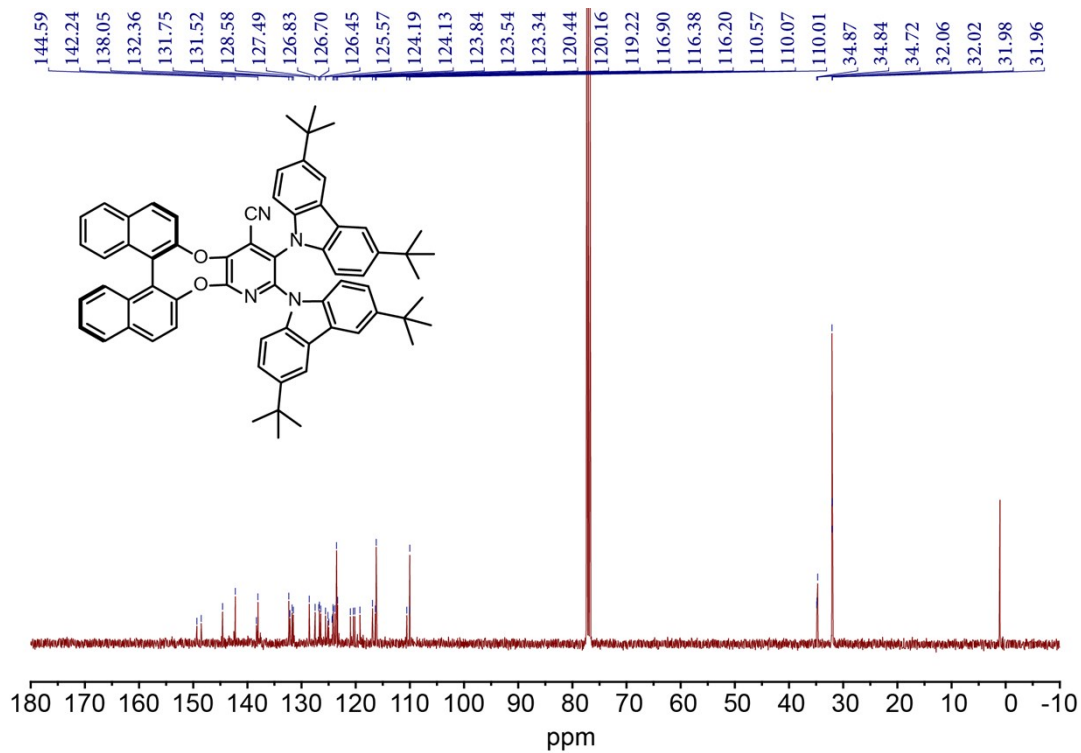


Figure S10. ^{13}C NMR spectrum of **S-CPDCB** in CDCl_3 .

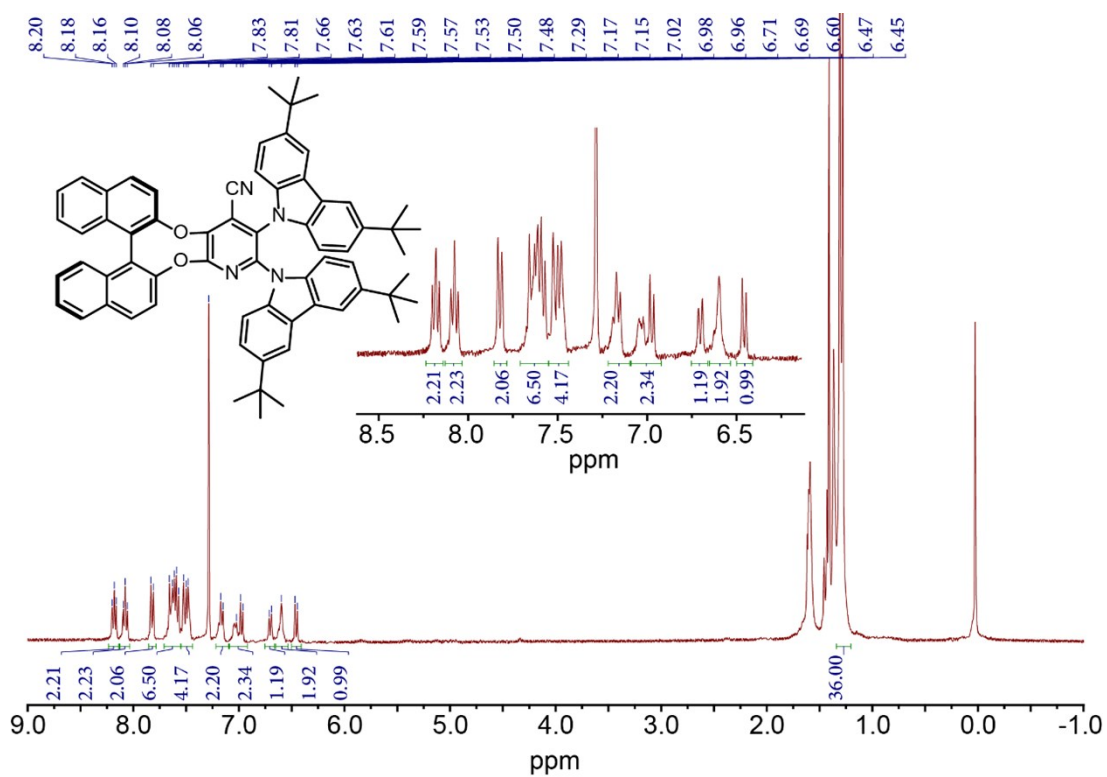


Figure S11. ^1H NMR spectrum of **R-CPDCB** in CDCl_3 .

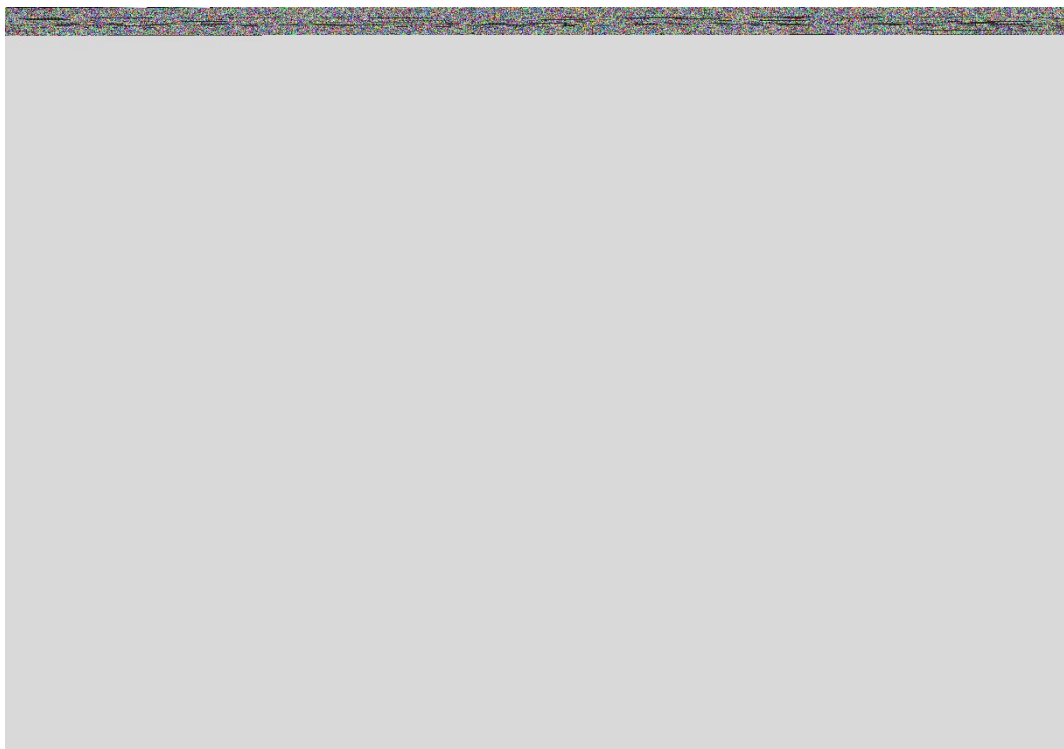


Figure S12. ^{13}C NMR spectrum of **R-CPDCB** in CDCl_3 .

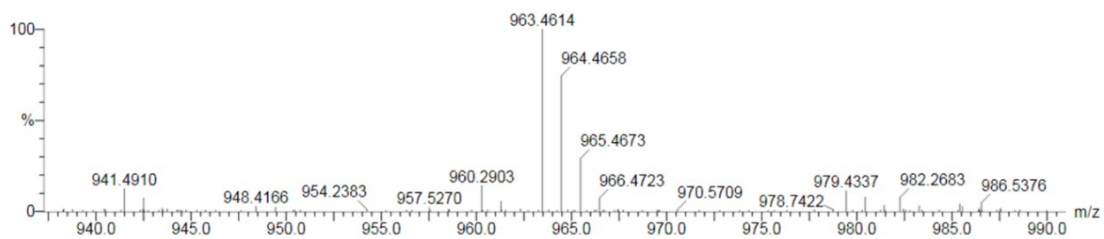


Figure S13. HRMS spectrum of **S-CPDCB**.

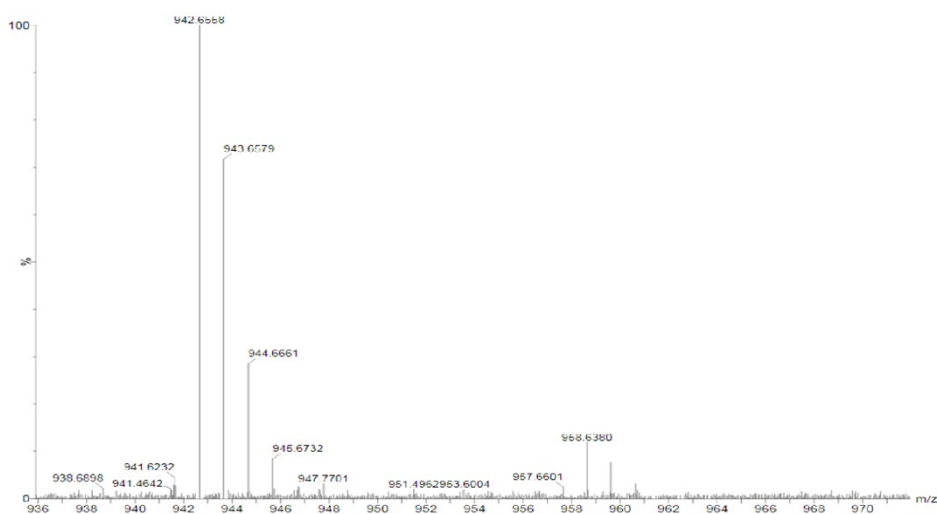


Figure S14. HRMS spectrum of **R-CPDCB**.

The isolated intermediates of 2,3-difluorodinaphtho[2',1':5,6;1'',2'':7,8][1,4]dioxocino[2,3-b]pyridine-4-carbonitrile (S-/R-CPDF)

The intermediates of **S-CPDF** and **R-CPDF** can be also isolated separately. Take **S-CPDF** as an example. A mixture of [1,1'-binaphthalene]-2,2'-diol (**S-BINOL**) (1.6 g, 5.60 mmol), 2,3,5,6-tetrafluoropyridine-4-carbonitrile (1.0 g, 5.60 mmol) and K₂CO₃ (3.0 g, 22.40 mmol) was dissolved in anhydrous N,N-dimethylformamide (DMF) (50 mL). The mixture was stirred for 12 h at room temperature to complete the reaction. Then water (80 mL) was added to quench the reaction. The resulting mixture was extracted with ethyl acetate (3×40 mL). The organic layers were combined and dried with anhydrous Na₂SO₄ and evaporated under reduced pressure to remove the solvents. The residue was purified by silica gel column chromatography (petroleum ether/dichloromethane = 3:1) to yield 1.54 g (65%) of the product as a white powder of **S-CPDF**: ¹H NMR (400 MHz, CDCl₃): δ = 8.10-8.06 (*t*, J = 16 Hz, 2H), 8.03-8.00 (*m*, 2H), 7.61-7.51 (*m*, 5H), 7.49-7.41 (*m*, 3H); ¹³C NMR (100 MHz, CDCl₃): δ = 149.98, 148.49, 146.92, 146.80, 145.36, 143.25, 142.94, 142.23, 140.22, 132.34, 132.06, 131.67, 131.53, 128.55, 127.53, 127.47, 126.79, 126.62, 126.52, 126.42, 125.11, 124.95, 120.67, 120.25, 109.09, 108.59, 108.55. Yield: 1.47 g of **R-CPDF** in white powder (62%): ¹H NMR (400 MHz, CDCl₃): δ = 8.10-8.06 (*t*, J = 16 Hz, 2H), 8.03-8.00 (*m*, 2H), 7.61-7.51 (*m*, 5H), 7.49-7.41 (*m*, 3H); ¹³C NMR (100 MHz, CDCl₃): δ = 149.98, 148.49, 146.92, 146.80, 145.36, 143.25, 142.94, 142.43, 140.22, 132.34, 132.25, 132.06, 131.67, 131.53, 128.55, 127.53, 127.47, 126.79, 126.62, 126.52, 126.42, 125.11, 124.95, 120.67, 120.25, 109.09, 108.59, 108.55.

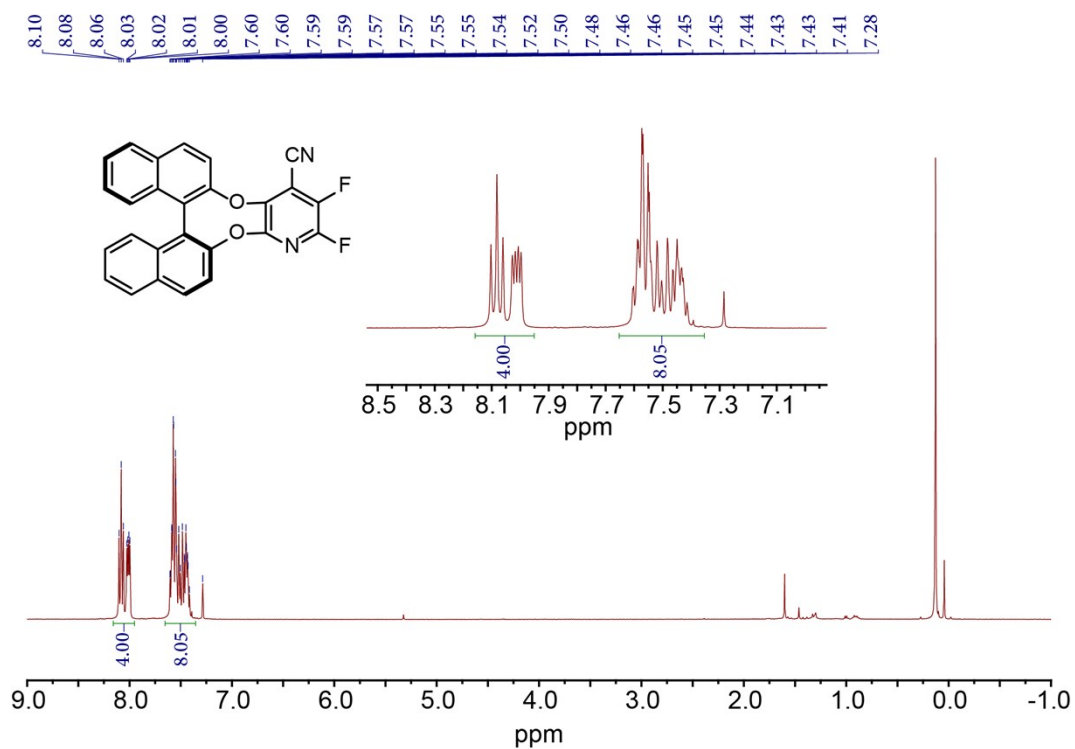


Figure S15. ¹H NMR spectrum of S-CPDF in CDCl₃.

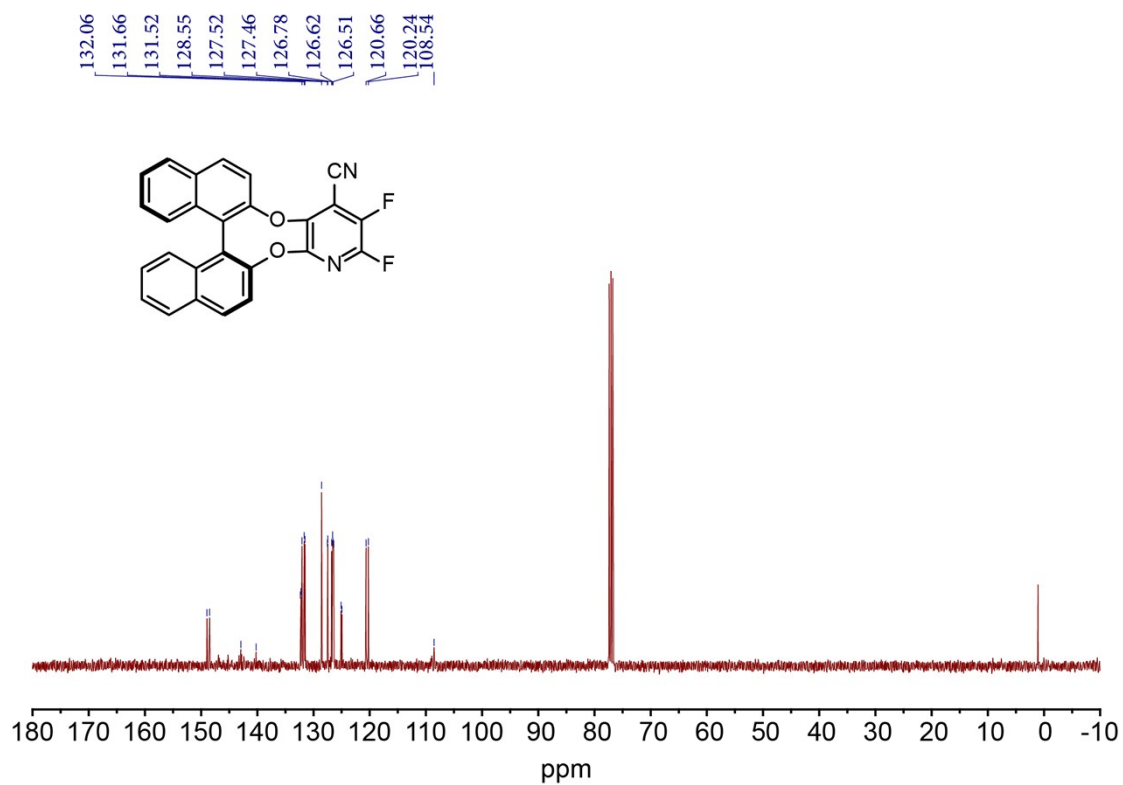


Figure S16. ¹³C NMR spectrum of S-CPDF in CDCl₃.

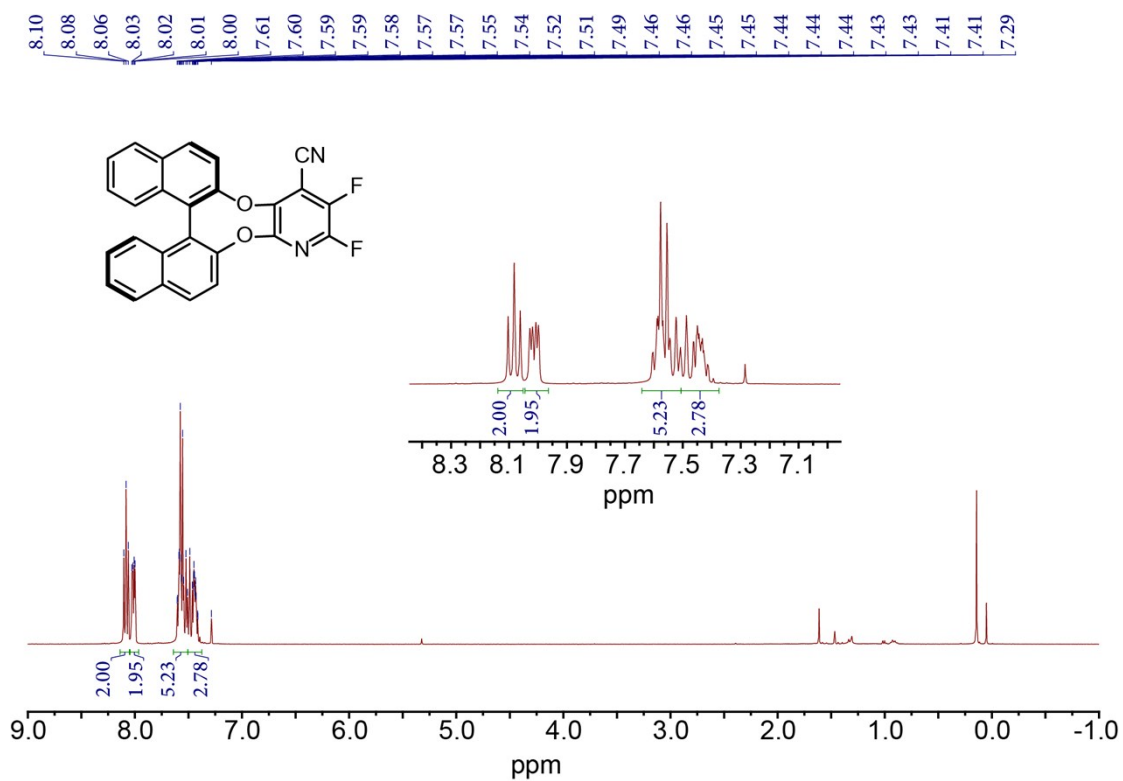


Figure S17. ^1H NMR spectrum of **R-CPDF** in CDCl_3 .

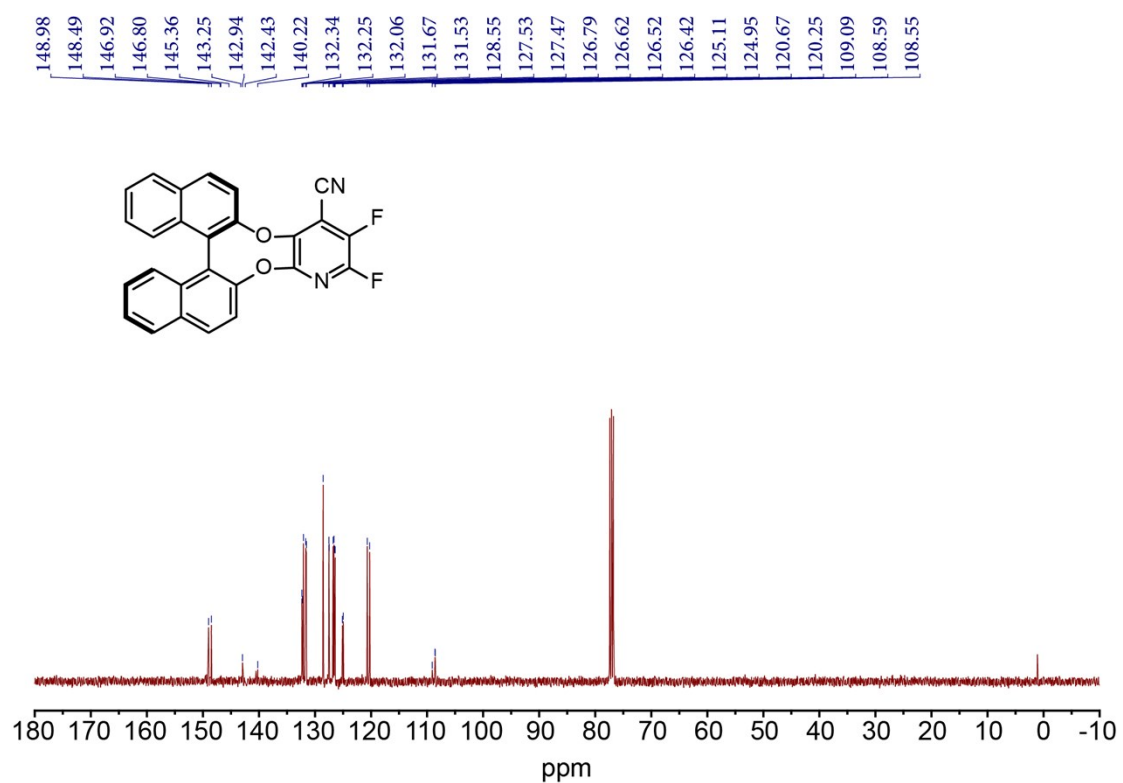


Figure S18. ^{13}C NMR spectrum of **R-CPDF** in CDCl_3 .

3. Chiral high-performance liquid chromatography (HPLC) analysis

Chiral HPLC analysis was used to investigate the enantiomeric excess of the chiral molecules after the synthetic and purification procedures. HPLC analysis conditions are as follows. The column is CHIRALCEL IA chiral column (250 mm × 4.6 mm × 5 μm), and the mobile phase is hexane: dichloromethane = 50:50 (v:v) at a flow rate of 1.0 mL/min using an absorption detector at 300 nm (Figures S19-20).

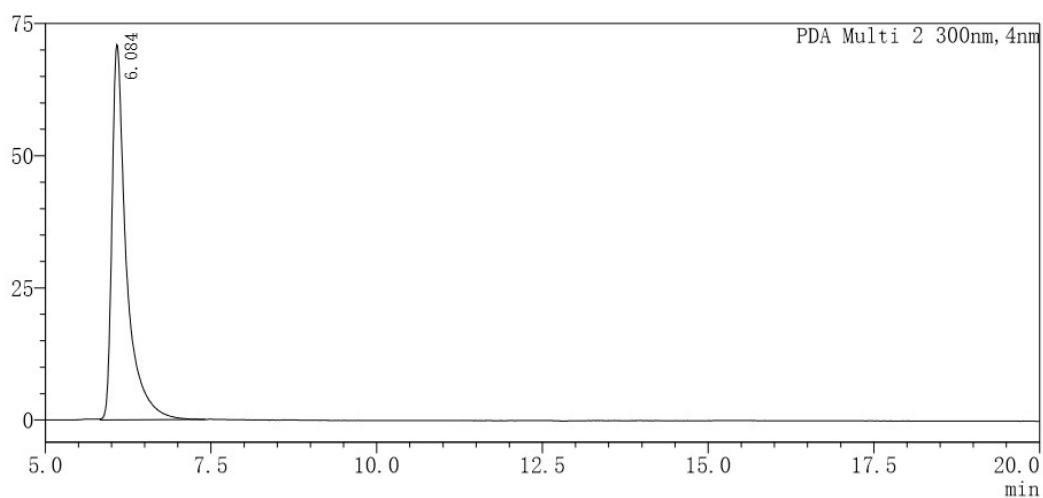


Figure S19. Chiral HPLC chromatogram of **S-CPDCz**.

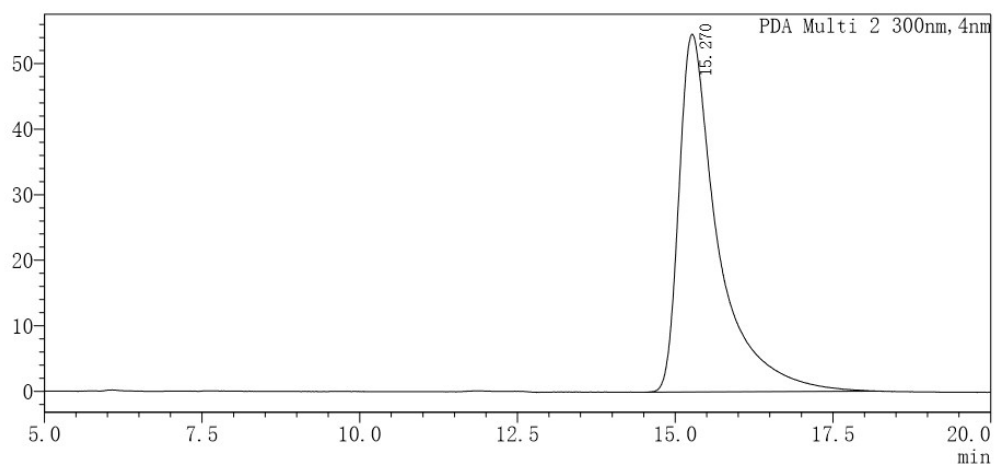


Figure S20. Chiral HPLC chromatogram of **R-CPDCz**.

4. Thermal properties

Thermogravimetric analyses (TGA) were conducted on a DTG-60 Shimadzu thermal analyst system under a heating rate of 10°C/min and a nitrogen flow rate of 50 cm³/min. The differential scanning calorimetry (DSC) analyses were performed on a Shimadzu DSC-60A instrument under a heating rate of 10°C/min and a nitrogen flow rate of 20 cm³/min. Thermal decomposition temperature (T_d) is defined as the temperature when the sample's weight loss reaches 5%.

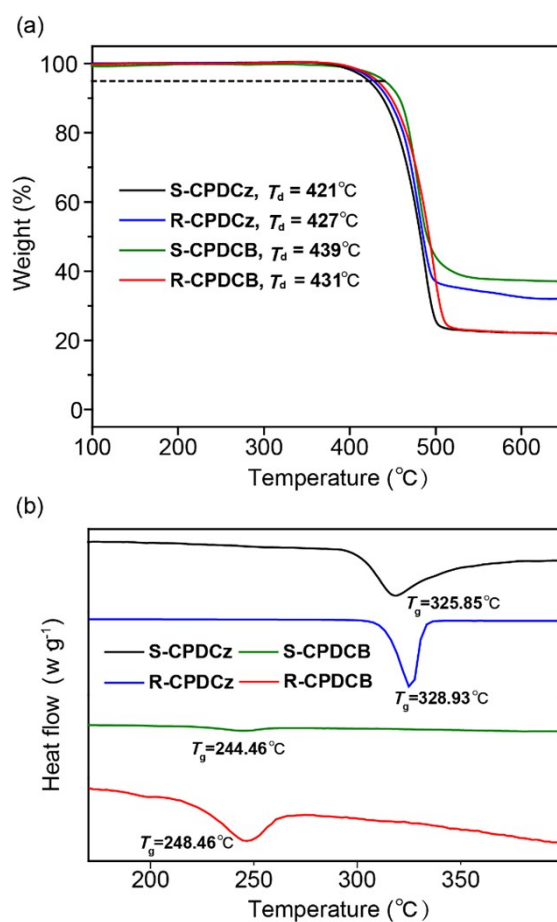


Figure S21. (a) TGA and (b) DSC plots of S/R-CPDCz and S/R-CPDCB.

5. Theoretical calculations

Density functional theory (DFT) and time-dependent DFT (TD-DFT) calculations were carried out on Gaussian 09 D.01 package^[2a]. The ground state geometry was fully optimized at B3LYP/6-31G(d) level and the optimized stationary point was further

characterized by harmonic vibration frequency analysis to ensure that real local minima had been found. Using the overlap integral function embedded in Multiwfn,^[2b] the overlap between two orbitals (φ_i and φ_j) of a molecule can be calculated according to

Equation S1:

$$I = \int \varphi_i(r) \varphi_j(r) dr \quad (\text{S1})$$

Therefore, the extents of HOMO (φ_H) and LUMO (φ_L) overlap were obtained using

Equation S2:

$$I_{HL} = \int \varphi_H(r) \varphi_L(r) dr \quad (\text{S2})$$

6. Morphology properties

Atomic force microscopy (AFM) measurements were carried out at room temperature using a Bruker Dimension Icon AFM equipped with Scanasyst-Air peak force tapping mode AFM tips from Bruker. The thin films were prepared through spin-coating on glass substrates under the identical conditions as that in device fabrication. The RMS in the figure represents root mean square.

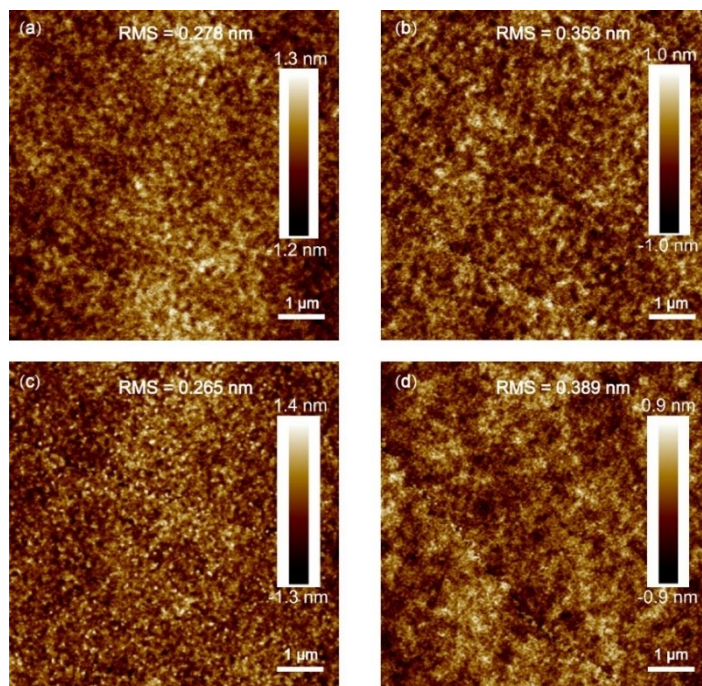


Figure S22. Atomic Force Microscope images of (a) **S-CPDCz**, (b) **R-CPDCz**, (c) **S-CPDCB**, and (d) **R-CPDCB** doped in 1,3-Bis(carbazol-9-yl) benzene (mCP) film (10 wt%).

7. Photophysical properties

Ultraviolet/visible (UV/vis) absorption and photoluminescence (PL) spectra were recorded on a Lambda 650 S Perkin Elmer UV/vis spectrophotometer and a LS 55 Perkin Elmer, respectively. The time-resolved phosphorescence spectra were obtained using an Edinburgh FLS 920 fluorescence spectrophotometer at 77 K with a 5 ms delay time after the excitation using a microsecond (μ s) flash lamp.

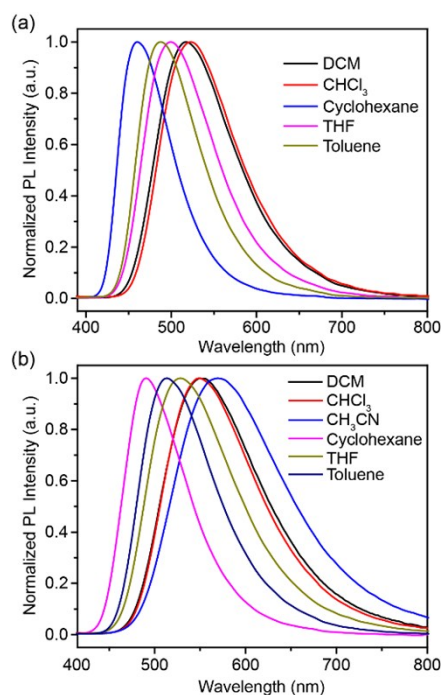


Figure S23. PL spectra of (a) **S-CPDCz** and (b) **S-CPDCB** in different solvents (conc. $\sim 10^{-5}$ M).

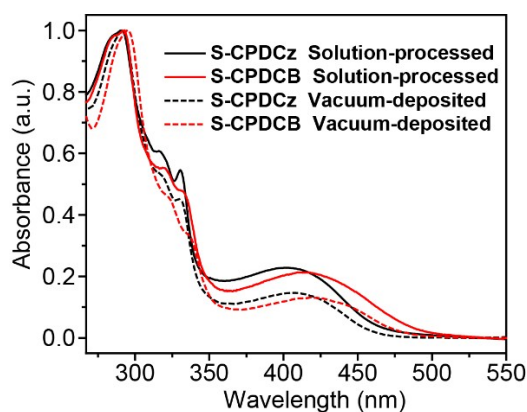


Figure S24. UV-vis absorption spectra of **S-CPDCz** and **S-CPDCB** in vacuum-deposited and solution-processed films at room temperature.

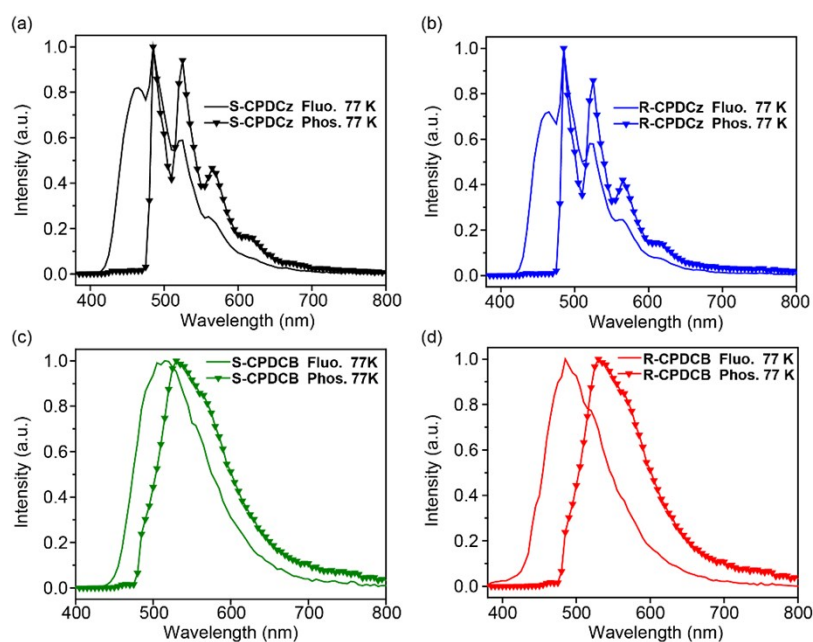


Figure S25. Fluorescence and phosphorescence spectra of (a) **S-CPDCz**, (b) **R-CPDCz**, (c) **S-CPDCB**, and (d) **R-CPDCB** in THF (conc. 10^{-5} M) at 77 K. The phosphorescence was collected with a delay time of 5 ms.

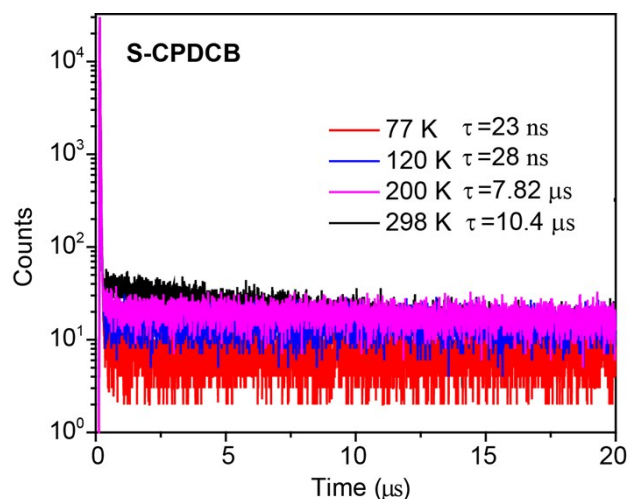


Figure S26. Temperature dependence transient PL (533 nm) characteristics of the chiral TADF molecules doped in mCP films (10 wt%) at different temperatures. Inset: The curve of lifetime changes with temperature.

Table S1. Photophysical properties of **R/S-CPDCz** and **R/S-CPDCB**.

Guest	Absorption (nm)		E_g^a (eV)	PL (nm)		g_{lum}^b	
	THF	Film		THF	Film	CH ₂ Cl ₂	Film
R-CPDCz	289, 315, 396	290, 318, 406	2.70	503	516	3.3×10^{-4}	3.7×10^{-4}
S-CPDCz	289, 315, 396	290, 318, 406	2.71	500	511	-3.0×10^{-4}	-3.3×10^{-4}
R-CPDCB	289, 319, 410	294, 321, 417	2.66	527	529	3.2×10^{-4}	5.8×10^{-4}
S-CPDCB	392, 322, 415	294, 321, 417	2.67	530	533	-2.1×10^{-4}	-4.0×10^{-4}

a) Optical band gap (E_g) was calculated by the absorption edge technique in solid film.

b) g_{lum} of the four molecules in dilute THF (conc. 10^{-5} M) and thin film.

Table S2. Electrochemical and photophysical properties of **R/S-CPDCz** and **R/S-CPDCB**.

Guest	HOMO (eV)		LUMO (eV)		ΔE_{ST}^b (eV)	E_T (eV)		$\tau_{delayed}^d$ (μ s)	PLQY ^e (%)	
	Cal.	Exp.	Cal.	Exp. ^a		Cal.	Exp. ^c		In THF	In mCP
R-CPDCz	-5.49	-5.84	-2.18	-2.87	0.08	2.44	2.60	15	27.8	20.0
S-CPDCz	-5.48	-5.82	-2.19	-2.87	0.08	2.44	2.60	18	27.4	20.0
R-CPDCB	-5.35	-5.70	-2.09	-2.86	0.03	2.35	2.62	8	37.0	55.0
S-CPDCB	-5.34	-5.67	-2.07	-2.85	0.04	2.34	2.61	10	37.1	55.2

a) Estimated by adding E_g to the HOMO energy level. b) Calculated using $\Delta E_{ST} = E_{S1} - E_{T1}$. c) Measured from the phosphorescent spectrum. d) Delayed fluorescence lifetime evaluated in doped film (mCP, 10 wt%) at room temperature. e) In dilute THF solution (10^{-5} mol/L) and mCP film (10 wt%) using an integrating sphere.

8. Electrochemical properties

Cyclic voltammetry (CV) measurements were performed at room temperature on a CHI660E system in a typical three-electrode cell with a working electrode (glass carbon), a reference electrode (Ag/Ag^+), referenced against ferrocene/ferrocenium (FOC) and a counter electrode (Pt wire). The electrochemical experiments were carried out in an acetonitrile solution of Bu_4NPF_6 (0.1 M) at a sweeping rate of 100 mV s^{-1} . The highest occupied molecular orbital (HOMO) energy levels (E_{HOMO}) of the materials deposited as thin films on the surface of the working electrode were measured according to the reference energy level of ferrocene (4.8 eV below the vacuum) as illustrated in **Equation S1**^[3]:

$$E_{\text{HOMO}} = -[E_{\text{onset}}^{\text{Ox}} - E_{(\text{Fc}/\text{Fc}^+)} + 4.8] \text{ eV} \quad (\text{S2})$$

where $E_{(\text{Fc}/\text{Fc}^+)}$ is the onset oxidative voltage of FOC vs Ag/Ag^+ and $E_{\text{onset}}^{\text{Ox}}$ is the onset potential of the oxidation wave. The lowest unoccupied molecular orbital (LUMO) energy level (E_{LUMO}) was estimated by adding the optical band-gap (E_g) to the corresponding HOMO energy level as in **Equation S2**^[4]:

$$E_{\text{LUMO}} = [E_{\text{HOMO}} + E_g] \text{ eV} \quad (\text{S3})$$

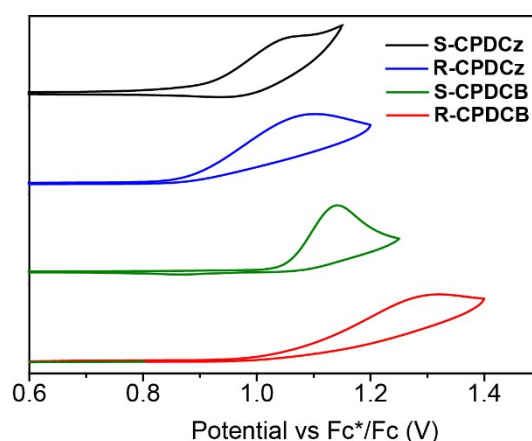


Figure S27. Cyclic voltammograms of S/R-CPDCz and S/R-CPDCB.

9. Thermally activated delayed fluorescence organic light emitting diode (TADF OLED)

9.1 Materials and device structures

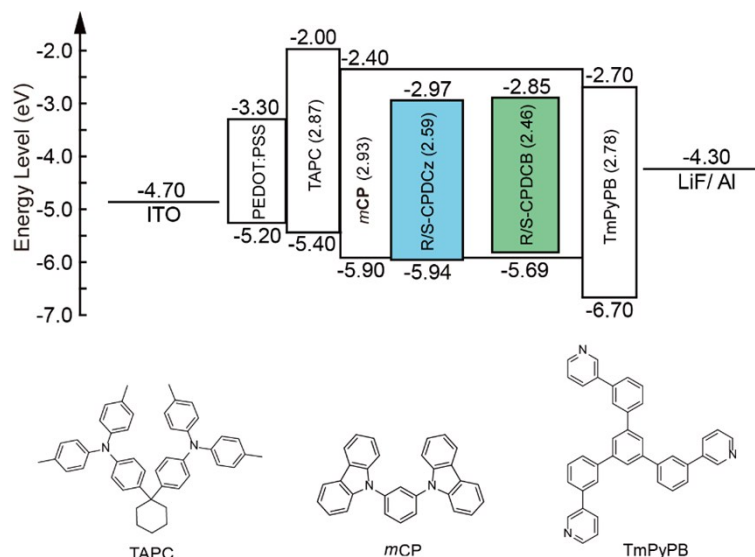


Figure S28. Energy level diagram and device architecture of the vacuum-deposited TADF CP-OLEDs with the chemical structures of the materials used.

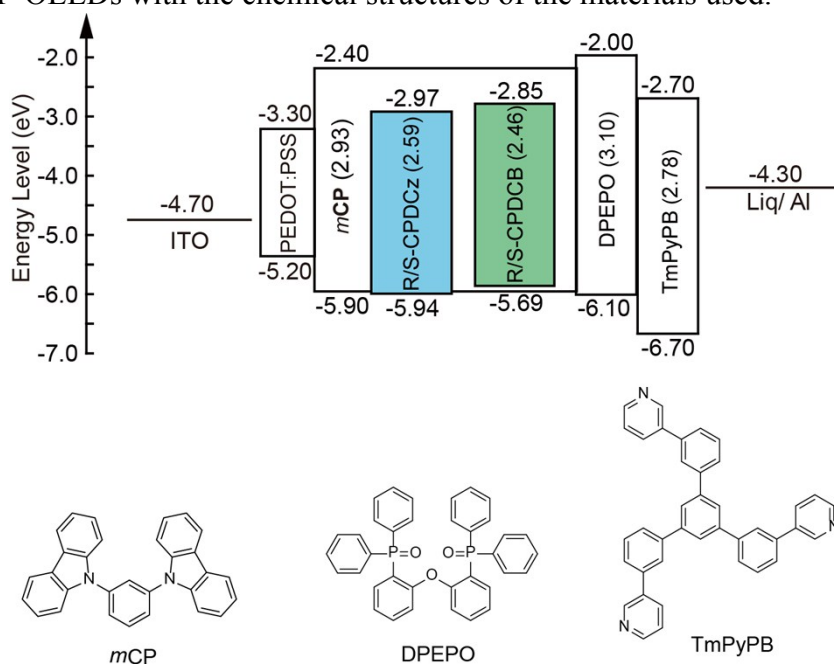


Figure S29. Energy level diagram and device architecture of the solution-processed TADF CP-OLEDs with chemical structures of the related materials.

9.2 Device fabrication and measurements

The vacuum-deposited TADF OLEDs were fabricated as follows. The hole-injection material of poly(3,4-ethylenedioxythiophene): poly (styrene sulfonic acid) (PEDOT: PSS) was purchased from H.C. Starck. The hole-transporting material of 4,4'-cyclohexylidenebis[N,N-bis(4-methylphenyl)aniline] (TAPC), the electron-transporting material of 1,3,5-tri(m-pyrid-3-yl-phenyl)-benzene (TmPyPB), the host material of mCP, lithium fluoride (LiF) as the electron injection layer, and aluminum functions as the cathode were used as-received without further purification. TADF OLED devices were prepared in the following procedure.^[5] The patterned indium-tin oxide (ITO) glass substrates were ultrasonically cleaned with detergent, alcohol, acetone, and deionized water for 30 min respectively, and then dried at 120°C in a vacuum oven for more than one hour. After ultraviolet (UV)-ozone treating for 15 min, the samples were transferred to a thermal evaporator chamber. Then, the PEDOT: PSS was spin coated on the ITO substrate and dried at 120°C in a vacuum oven for 15 min, TAPC (20 nm), emissive layers (EMLs), TmPyPB (30 nm), LiF (1 nm), and Al (100 nm) were deposited subsequently by thermal evaporation under a pressure of 5×10^{-4} Pa. Organic materials were deposited at a rate of $1-2 \text{ \AA s}^{-1}$ and the deposition rates of LiF and Al were 0.1 and 10 \AA s^{-1} , respectively.

The thicknesses of the layers, monitored in situ by an oscillating quartz thickness monitor, were confirmed by a spectroscopic ellipsometry (α -SE, J.A. Wollam Co. Inc.) or a Bruker Dektak XT stylus profiler. The active area of the device was controlled to be 9 mm^2 . Devices without encapsulation were measured at room temperature under ambient atmosphere conditions. The luminance-current-voltage (L-J-V) characteristics of the devices were recorded by a Keithley source-meter (model 2602) and a calibrated luminance meter. Electroluminescence (EL) spectra were obtained using a spectra-scan PR655 spectrophotometer.

The solution-processed TADF OLEDs were fabricated as follows. The hole-blocking material of Bis[2-[(oxo)diphenylphosphino]phenyl] Ether (DPEPO), The electron-transporting material of TmPyPB, the host material of mCP, electron-injection

material of 8-hydroxyquinolinolato-lithium (Liq), and aluminum functions as the cathode. All the above-mentioned materials were used as-received without further purification. TADF OLED devices were prepared in the following procedure. The patterned ITO glass substrates were ultrasonically cleaned with detergent, alcohol, acetone, and deionized water for 30 min respectively, and then dried at 120°C in a vacuum oven for more than one hour. After ultraviolet (UV)-ozone treating for 15 min, a 30 nm PEDOT: PSS was spin coated on the ITO substrate and dried at 120°C in a glove-box for 10 min. Then, the emissive layers (EMLs) were spin-coated on the top of PEDOT: PSS from chlorobenzene (10 mg mL⁻¹) and annealed using a hot plate at 50°C for 10 min. After that, the samples were transferred to a thermal evaporator chamber. DPEPO (10nm), TmPyPB (50 nm), Liq (1 nm), and Al (100 nm) were deposited subsequently by thermal evaporation under a pressure of 5×10⁻⁴ Pa.

The thickness of the TADF OLED layers was monitored using a Bruker Dektak XT stylus profiler. The active area of the devices is 4.4 mm². The devices encapsulated with UV epoxy were measured immediately after fabrication at room temperature under ambient atmosphere conditions. The luminance-current-voltage (L-J-V) characteristics of the devices were recorded by a combination of a Keithley source-meter (model 2602) and a calibrated luminance meter. Electroluminescence (EL) spectra were obtained using a spectra scan PR735 spectrophotometer. The external quantum efficiency (EQE) was achieved according to **Equation S3**^[6].

$$EQE = \frac{\pi e \eta_{cd/A} / A \int \lambda P(\lambda) d\lambda}{hc K_m \int \lambda P(\lambda) d\lambda} \quad (S5)$$

where $\eta_{cd/A}$ is the current efficiency (in cd/A); h is the Planck constant; c is the speed of light in vacuum; λ is the wavelength (in nm); e is the electron charge; $p(\lambda)$ is relative electroluminescent intensity at each wavelength; $\Phi(\lambda)$ is the commission international de l'Eclairage chromaticity (CIE) standard photopic luminous efficiency function; and K_m is a constant of 683 lm/W.

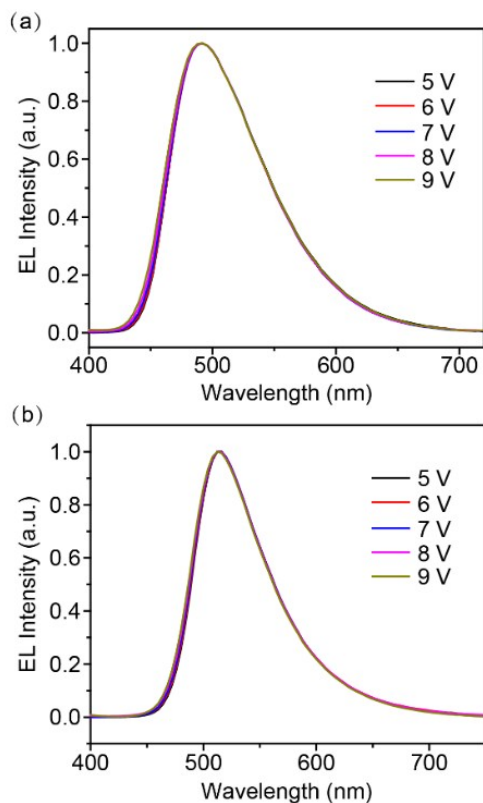


Figure S30. Electroluminescence (EL) spectra at different driving voltages of the vacuum-deposited TADF CP-OLEDs based on (a) S/R-CPDCz and (b) S/R-CPDCB.

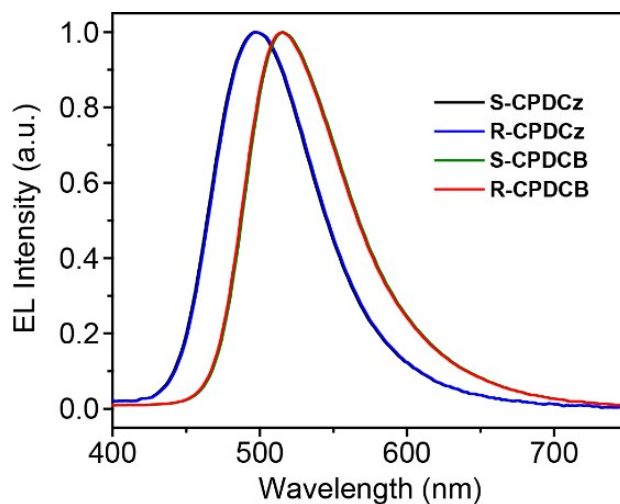


Figure S31. Electroluminescence (EL) spectra of S/R-CPDCz and S/R-CPDCB of the solution-processed TADF CP-OLEDs.

10. CPL and CPEL measurements

Circularly polarized luminance (CPL) and circularly polarized

electroluminescence (CPEL) spectra were recorded on JASCO CPL-300 at room temperature under a driving voltage of 9.0 V in atmosphere.

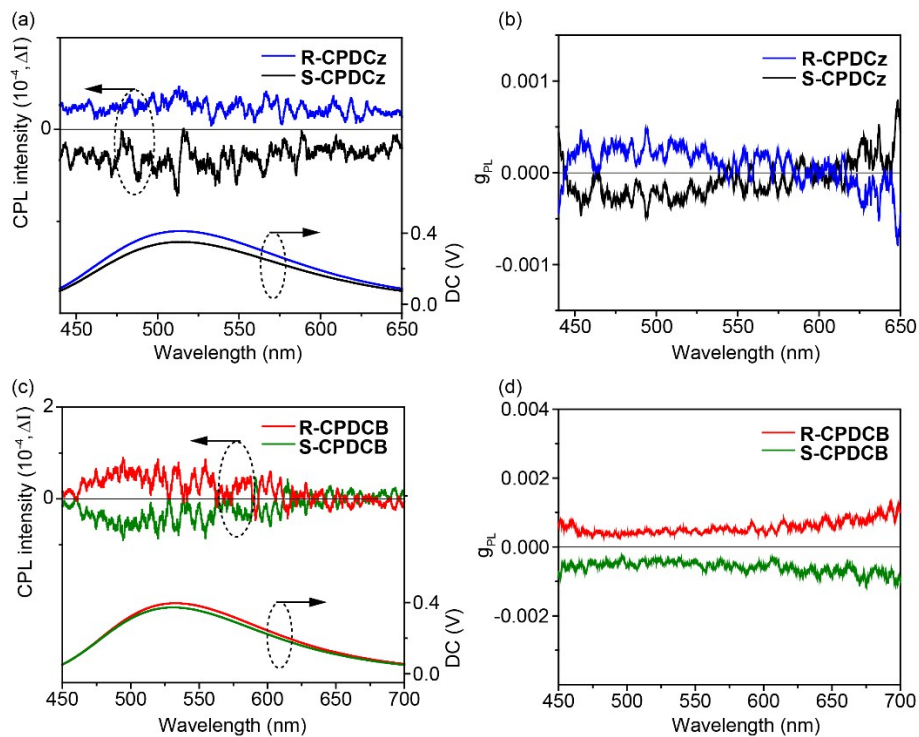


Figure S32. (a, c) CPL spectra and (b, d) g_{PL} values of the vacuum-deposited R/S-CPDCz (10 wt%): mCP and R/S-CPDCB (10 wt%): mCP films.

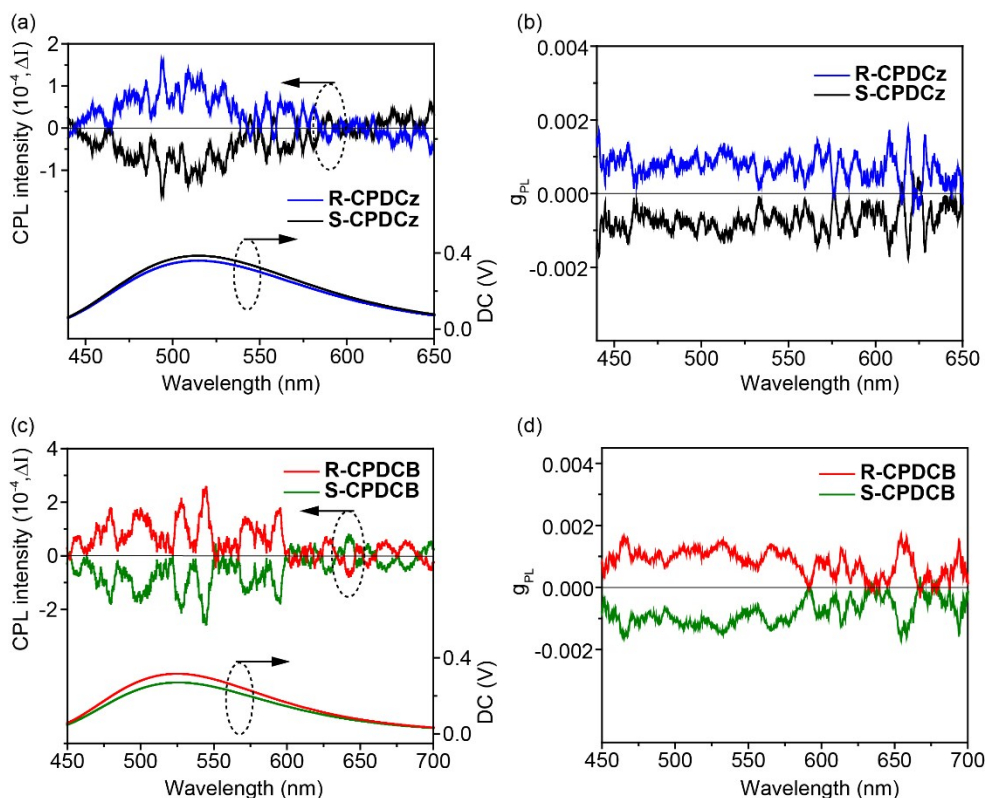


Figure S33. (a, c) CPL spectra and (b, d) g_{PL} values of the spin-coated **R/S-CPDCz** (10 wt%): mCP and **R/S-CPDCB** (10 wt%): mCP films.

Table S3: g_{PL} values of the vacuum-deposited and the spin-coated **R/S-CPDCz** (10 wt%): mCP and **R/S-CPDCB** (10 wt%): mCP films.

Compound	Method	g_{PL}
R/S-CPDCz	Solution-processed	$7.64 \times 10^{-4} / -7.70 \times 10^{-4}$
R/S-CPDCB	Solution-processed	$9.93 \times 10^{-4} / -9.92 \times 10^{-4}$
R/S-CPDCz	Vacuum-deposited	$4.68 \times 10^{-4} / -4.52 \times 10^{-4}$
R/S-CPDCB	Vacuum-deposited	$4.64 \times 10^{-4} / -4.65 \times 10^{-4}$

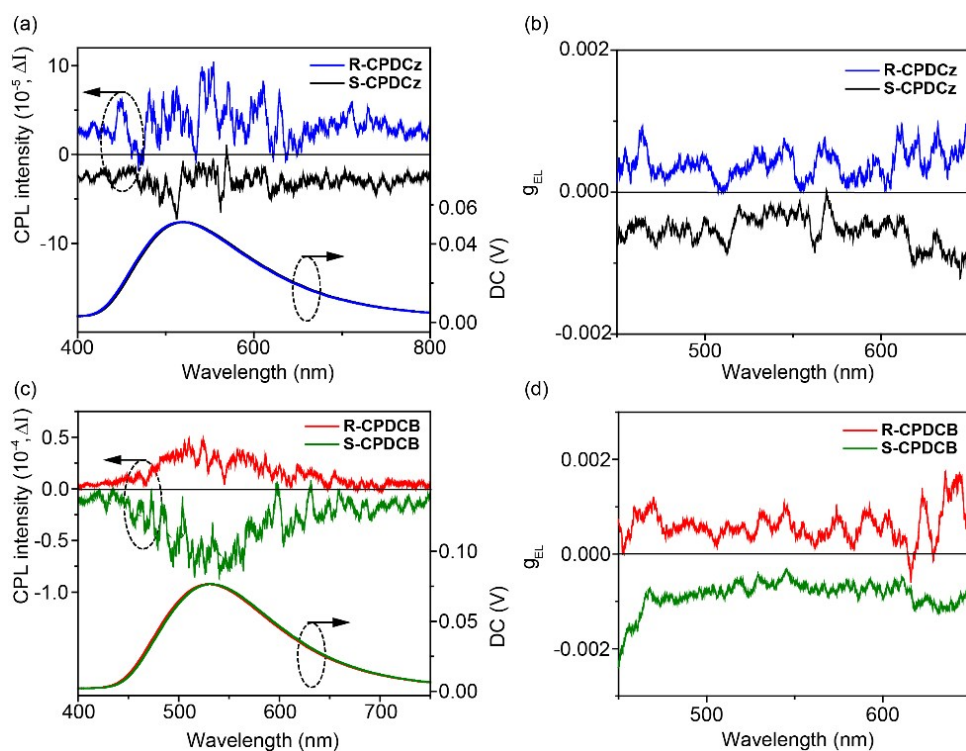


Figure S34. (a, c) CPEL and (b, d) g_{EL} spectra of (a, b) S/R-CPDCz and (c, d) S/R-CPDCB at the maximum EL wavelength of the vacuum-deposited CP-OLEDs.

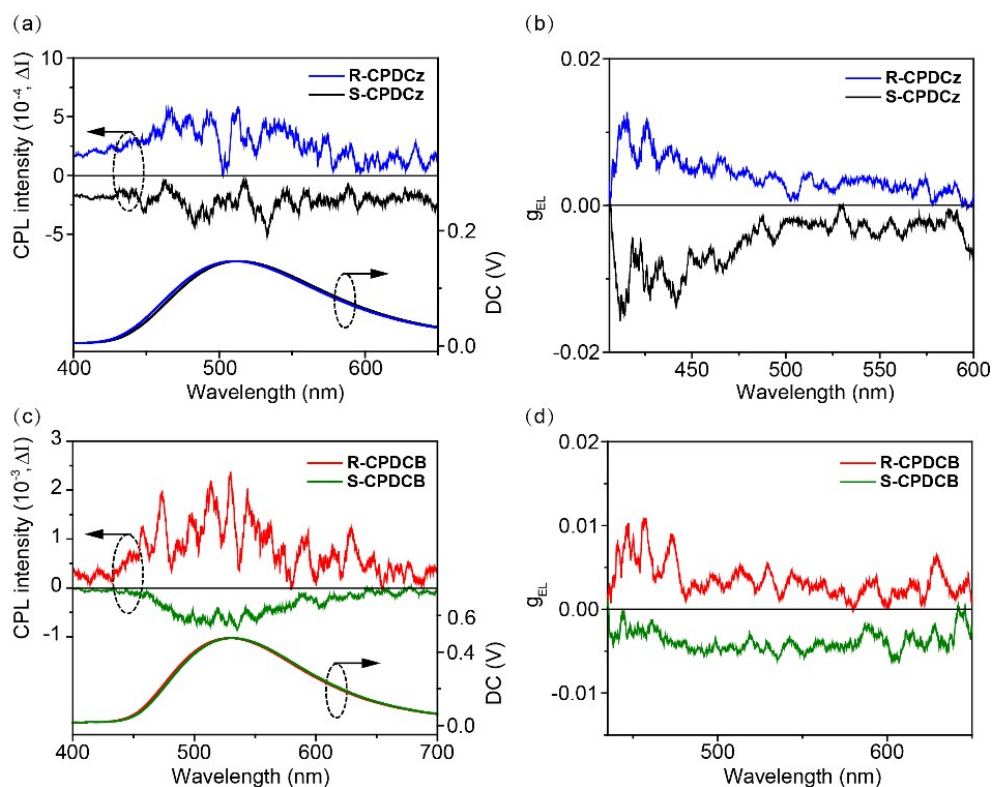


Figure S35. (a, c) CPEL and (b, d) g_{EL} spectra of (a, b) S/R-CPDCz and (c, d) S/R-CPDCB at the maximum EL wavelength in solution-processed CP-OLEDs.

11. A summary of CP-OLEDs

Table S4. Device performance of the CP-OLEDs based on chiral fluorescent (FI), phosphorescent (Ph), and TADF molecules using different fabrication methods.

Comp.	Fabrication Method	Type	V (V)	λ_{\max} (nm)	L_{\max} (cd m ⁻²)	CE (cd A ⁻¹) ^{a)}	PE (lm W ⁻¹) ^{a)}	EQE (%) ^{a)}	g_{EL}	References
S-BN-AF	Vacuum	TADF OLED	4.0	571	3032	4.2	2.9	1.7	0.084	[1]
S-BN-DCB	Vacuum	TADF OLED	3.4	547	5056	10.5	9.1	3.5	0.067	[1]
S-BN-CCB	Vacuum	TADF OLED	3.6	527	4199	20.9	18.2	6.3	0.054	[1]
(R)-1	Vacuum	TADF OLED	4.0	550	-	34.7	16.3	9.1	-	[7]
S-BN-CF	Vacuum	TADF OLED	3.6	496	2948	24.6	19.6	9.3	0.06	[1]
D-D(S)	Vacuum	TADF OLED	3.9	550	24518	45.3	30.6	12.4	-0.0018	[8]
CzPPhTrz	Vacuum	TADF OLED	3.2	480	-	34.8	32.5	17.0	-	[9]
(P/M)-Pt	Vacuum	Ph-OLED	3.4	600	11590	22.52	18.62	18.8	1.4×10^{-3}	[10]
(S, S)-Cal-Cz	Vacuum	TADF OLED	3.4	520	3000	59.0	53.0	19.7	-1.7×10^{-3}	[11]
(R, R)-Cal-Cz	Vacuum	TADF OLED	3.4	520	7000	59.4	52.9	19.8	-1.7×10^{-3}	[11]
(R-)Ir(ppy)₂(acac)	Vacuum	Ph-OLED	3.2	520	135676	103.5	88.29	28.0	-	[12]
R-OBN-Cz	Vacuum	TADF OLED	3.8	500	35633	95.3	60	32.6	2.34×10^{-3}	[13]
S-CPDCB	Vacuum	TADF OLED	3.70	515	7700	39.5	30.3	12.4	-8.6×10^{-4}	This work
S-CPDCz	Vacuum	TADF OLED	3.80	492	3700	21.4	15.7	8.4	-5.5×10^{-4}	This work
S1	Solution	Ph-OLED	6.5	557	3788	6.47	2.55	-	$+3.0 \times 10^{-3}$	[14]
R1	Solution	Ph-OLED	6.5	558	4473	6.08	2.38	-	$+2.3 \times 10^{-3}$	[14]
R-6	Solution	FI-OLED	3.26	540	7946	1.26	-	0.45	-3.0×10^{-3}	[15]
S-6	Solution	FI-OLED	3.18	530	8061	1.32	-	0.48	$+3.2 \times 10^{-3}$	[15]
S-CPDCB	Solution	TADF OLED	3.60	516	1785	33.3	26.1	10.6	-3.9×10^{-3}	This work
S-CPDCz	Solution	TADF OLED	3.60	496	923	24.6	19.3	10.1	-3.7×10^{-3}	This work

^{a)}Maximum efficiencies.

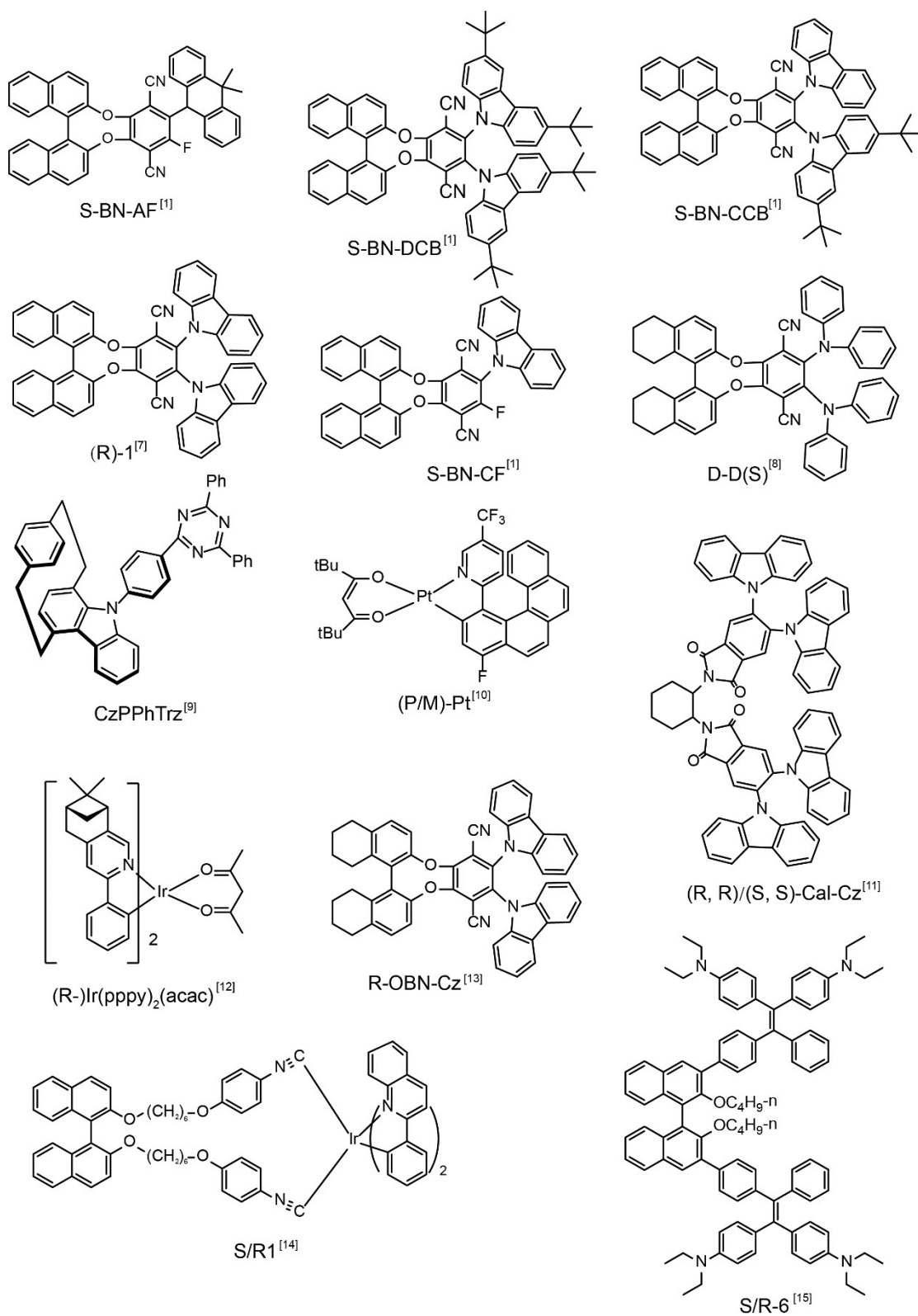


Figure S36. Molecular structures of the chiral emitters used in the CP-OLEDs listed in Table S4.

References

- [1] Song, F., Xu, Z., Zhang, Q., Zhao, Z., Zhang, H., Zhao, W., Qiu, Z., Qi, C., Zhang, H., Sung, H. H. Y., Williams, I. D., Lam, J. W. Y., Zhao, Z., Qin, A., Ma, D., Tang, B. Z. *Adv. Funct. Mater.* 2018, **28**, 1800051.
- [2] (a) Frisch, M. J. et al, Gaussian 09, revision D. 01, Gaussian, Inc Wallingford, CT, 2009. (b) Lu, T. Multiwfn: a multifunctional wavefunction analyzer version 3.3.3, 2013.
- [3] Yang, Y., da Costa, R. C., Smilgies, D.-M., Campbell, A. J., & Fuchter, M. J. *Adv. Mater.* 2013, **25**, 2624.
- [4] Liu, X.-Y., Liang, F., Ding, L., Li, Q., Jiang, Z.-Q., & Liao, L.-S. *Dyes pigm.* 2016, **126**, 131.
- [5] Liu, Y., Xie, G., Wu, K., Luo, Z., Zhou, T., Zeng, X., Yu, J., Gong, S., Yang, C. *J. Mater. Chem. C.* 2016, **4**, 4402.
- [6] Tao, Y., Guo, X., Hao, L., Chen, R., Li, H., Chen, Y., Zhang, X., Lai, W., Huang, W. *Adv. Mater.* 2015, **27**, 6939.
- [7] Feuillastre, S., Pauton, M., Gao, L., Desmarchelier, A., Riives, A. J., Prim, D., Tondelier, D., Geffroy, B., Muller, G., Clavier, G., Pieters, G. *J. Am. Chem. Soc.* 2016, **138**, 3990.
- [8] Wu, Z.-G; Yan, Z.-P., Luo, X.-F., Yuan, L., Liang, W.-Q., Wang, Yi., Zheng, Y.-X., Zuo, J.-L., Pan, Y. *Journal of Materials Chemistry C*, 2019, **7**, 7045.
- [9] Sharma, N., Spuling, E., Mattern, C. M., Li, W., Fuhr, O., Tsuchiya, Y., Adachi, C., Brase, S., Samuel, I. D. W., Zysman-C, E. *Chem Sci*, 2019, **10**, 6689.
- [10] Yan, Z.-P., Luo, X.-F., Liu, W.-Q., Wu, Z.-G., Liang, X., Liao, K., Wang Y., Zheng, Y.-X., Zhou, L., Zuo, J.-L., Pan, Y., Zhang, H. *Chem. Eur. J.* 2019, **25**, 5672.
- [11] Li, M., Li, S.-H., Zhang, D., Cai, M., Duan, L., Fung, M.-K., & Chen, C.-F. *Angew. Chem. Int. ed.* 2018, **57**, 2889–2893.
- [12] Zhou, Y.-H., Xu, Q.-L., Han, H.-B., Zhao, Y., Zheng, Y.-X., Zhou, L., Zuo, J.-L., Zhang, H. *Adv. Optical Mater.* 2016, **4**, 1726–1731.

- [13] Wu, Z.-G., Han, H.-B., Yan, Z.-P., Luo, X.-F., Wang, Y., Zheng, Y.-X., Zuo, J.-L., Pan, Y. *Adv. Mater.* 2019, **31**, 1900524.
- [14] Han, J., Guo, S., Wang, J., Wei, L., Zhuang, Y., Liu, S., Zhao, Q., Zhang, X., Huang, W. *Adv. Optical Mater.* 2017, **5**, 1700359.
- [15] Zhang, X., Zhang, Y., Zhang, H., Quan, Y., Li, Y., Cheng, Y., & Ye, S. *Org. Lett.* 2019, **21**, 439-443.